

**SOME STUDIES ON ENGINE COMBUSTION, EMISSION, AND
SPRAY CHARACTERISTICS OF A CRDI DIESEL ENGINE
WITH VARIABLE NOZZLE GEOMETRY USING ANSYS**

A THESIS

SUBMITTED IN THE FULFILLMENT OF THE REQUIREMENTS
FOR THE AWARD OF THE DEGREE
OF

MASTER OF TECHNOLOGY
IN
THERMAL ENGINEERING

Submitted by

VAIBHAV SINGH

(2k19/THE/21)

Under the supervision of

**Dr. NAVEEN KUMAR
(PROFESSOR)**



**DEPARTMENT OF MECHANICAL ENGINEERING
DELHI TECHNOLOGICAL UNIVERSITY
(Formerly Delhi College of Engineering)
Bawana Road, Delhi-110042**

OCTOBER, 2021

DECLARATION

I hereby declare that the thesis titled “**Some Studies on Engine Combustion, Emission, and Spray Characteristics of a CRDI Diesel Engine with Variable Nozzle Geometry Using ANSYS**” is an original work carried out by me under the supervision of Dr. Naveen Kumar, Professor, Department of Mechanical Engineering, Delhi Technological University, Delhi. This thesis has been prepared in conformity with the rules and regulations of the Delhi Technological University, Delhi. The research work reported and results presented in the thesis has not been submitted either in part or full to any other University or institute for the award of any other diploma or degree.



Vaibhav Singh

M.Tech (Thermal Engineering)

2K19/THE/21

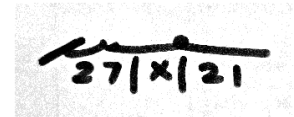
Date: 27/10/2021

Place: Delhi

CERTIFICATE

This is to certify that the work embodied in the thesis titled **“Some Studies on Engine Combustion, Emission, and Spray Characteristics of a CRDI Diesel Engine with Variable Nozzle Geometry Using ANSYS”** by **Vaibhav Singh**, (Roll No.: **2K19/THE/21**) in partial fulfilment of requirements for the award of Degree of **Master of Technology in Thermal Engineering**, is an authentic record of student’s own work carried by him under my supervision.

This is also certified that this work has not been submitted to any other University or institute for the award of any other diploma or degree.



Dr. Naveen Kumar
Professor

Mechanical Engineering Department
Delhi Technological University,
Delhi

**Dedicated to my Family & Friends whose constant support
helped me in completing this Research**

ACKNOWLEDGEMENT

The present research work was carried out under the esteemed supervision of my guide Prof. Naveen Kumar. It is my honor and privilege to express a deep sense of gratitude to him for his ever-helping attitude, critical and valuable comments, and constant inspiration. His mentorship helped me become a good researcher which I always dreamed of. His words of solace and encouragement especially during difficult times shall ever be remembered by me. I also acknowledge the blessing by Smt. Sumeeta Garg. I will be highly indebted to her for her affection.

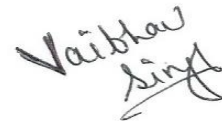
I owe gratitude to the esteemed colleagues of the Centre for Advanced Studies and Research in Automotive Engineering (CASRAE), Delhi Technological University; particularly my senior researchers Dr. Mukul Tomar, Mr. Dushyan Mishra, Mr. Hansham Dewal, and others for their excellent support and valuable suggestions.

I am thankful to Mr. Kamal Nain for providing all laboratory assistance. I am also thankful to Mr. Surendra Singh and Smt. Neetu Mishra, the supporting staff of CASRAE, DTU, Delhi.

I shall ever cherish the affection and blessings showered on me by my parents. Whatever I have achieved in my professional life; is all because of them. I cannot express in words their efforts put by them to nurture me. I am also indebted to my elder brother Mr. Himanshu who always extended

help whenever required. I place my sincere respect and a deep sense of gratitude on other family members. There are many more persons who have helped me directly or indirectly to complete this research work. I take this opportunity to thank all of them and apologize for their names not being here.

Last but not the least, I thank the Almighty for giving me the strength and patience to complete this work in all respects, leading to the path of success.

A handwritten signature in black ink that reads "Vaibhav Singh". The signature is written in a cursive style with a long horizontal stroke at the end of the name.

Vaibhav Singh
M.Tech (Thermal Engineering)
2K19/THE/21

ABSTRACT

The present study aims to investigate the effect on combustion, emission, and spray characteristics with the variation of the nozzle hole diameters (NHD) in a diesel engine. For this a CFD 3D model is developed for a four-stroke diesel engine fueled with neat diesel and three different NHD, i.e., 0.20 mm, 0.26 mm, and, 0.30 mm. The CFD 3D models were effectively able to predict the turbulence and turbulent-flame propagation interaction, chemistry involved in combustion processes, and the dissociation and reassociation of chemical species. For the model validation, the combustion characteristics of the CRDI-VCR engine are used. The validation results showed good compatibility having the relative error within the range. The analysis showed that increasing the nozzle hole diameter resulted in the decrease of the in-cylinder pressure by about 8.31% and 31.93%, respectively, for 0.26 mm and 0.30 mm diameter compared to 0.20 mm. The AHRR also showed a similar trend with a decrease of about 11.82% and 42.18%, respectively, for 0.26 mm and 0.30 mm diameter as compared to 0.20 mm. Subsequently, the increase in nozzle diameter showed an increase in HC and CO emissions but a decrease in NO_x emissions. The CO emissions increase by about 0.65% and 5.08% and HC emissions increase by about 29.90% and 60.13% respectively for 0.26 mm and 0.30 mm diameter compared to 0.20 mm.

While the NO_x emission reduces by about 41.18% and 70.58% respectively for 0.26 mm and 0.30 mm diameter as compared to 0.20 mm. The effect of different nozzle diameters on spray characteristics is analyzed and verified from previous studies. The increase in nozzle diameter showed an increase in liquid penetration length, breakup length, and SMD. Also, the present study shows the possibilities of the CFD models for the simulation of engines employing different fuels and operative conditions.

Keywords: *Nozzle hole diameter, Diesel engine, Ansys forte, Spray characteristics, NO_x emissions*

LIST OF CONTENTS

	Page No.
Declaration	ii
Certificate	iii
Dedication	iv
Acknowledgments	v
Abstract	vii
List of Contents	ix
List of Figures	xiii
List of Tables	xv
Nomenclature	xvi
CHAPTER 1 INTRODUCTION	1
1.1 Introduction	1
1.2 Combustion in CI Engine	3
1.3 Emissions in CI Engine	6
1.3.1 Un-burnt Hydrocarbons (UHC)	7
1.3.2 Carbon-monoxides (CO)	8
1.3.3 Nitrogen Oxides (NOx)	9
1.4 Diesel Spray Fundamentals	11
1.4.1 Atomization and Spray Development	13
1.4.2 Spray Penetration	14
1.4.3 Sauter Mean Diameter (SMD)	16
1.4.4 Spray Evaporation	19
1.5 Thesis Organization	21
CHAPTER 2 LITERATURE REVIEW	24
2.1 Introduction	24

2.2	Combustion and Performance Characteristics with Varying Nozzle Geometry	25
2.3	Emission Characteristics with Varying Nozzle Geometry	28
2.4	Spray Characteristics with Varying Nozzle Geometry	33
2.5	Summary	35
2.6	Research Gap	36
2.7	Objectives	36
CHAPTER 3	RESEARCH METHODOLOGY	37
3.1	Introduction	37
3.2	Basic Conservation Equations	37
	3.2.1 Turbulent Reacting Flows	37
	3.2.1.1 Species Conservation Equation	38
	3.2.1.2 Continuity Equation	39
	3.2.1.3 Momentum Conservation Equation	39
	3.2.1.4 Energy Conservation Equation	39
3.3	Turbulent Models	40
	3.3.1 Reynold-Average-Navier-Stokes (RANS) Model	40
	3.3.2 Large-Eddy-Simulation (LES) Model	42
	3.3.3 Formulation for Chemical Kinetics	43
	3.3.4 Turbulent-Kinetics Interaction Model	44
3.4	Discretization Methods	45
	3.4.1 Discretization-Governing Equations	45
	3.4.2 Temporal Differencing Method	45
	3.4.3 Spatial Differencing Method	46

3.5	SIMPLE Method	46
	3.5.1 Convective Flux Discretization	47
	3.5.2 Chemistry Solver	47
3.6	Spray and Break-up Models	47
	3.6.1 Nozzle Flow Model	48
	3.6.2 Kelvin-Helmholtz / Rayleigh-Taylor Break-up Model	49
	3.6.3 KH Break-up Model	50
3.7	Simulating a Diesel Engine	52
	3.7.1 Numerical Setup	52
	3.7.2 Initial and Boundary Conditions	53
	3.7.3 Grid Independence Test	54
3.8	Selection of Test Engine	55
3.9	Selection of Test Engine Parameters	57
	3.9.1 Measurement of Engine Power	58
	3.9.2 Measurement of Engine Speed	59
	3.9.3 Measurement of Fuel Consumption Rate	59
	3.9.4 Measurement of Temperature	59
	3.9.5 Measurement of In-cylinder Pressure	59
	3.9.6 Calculation of Heat Release Rate	60
3.10	Modification of Fuel Injection System (FIS)	61
3.11	Experimental Trial Procedure	63
	3.11.1 Test for Finding the Optimized Injection Duration	64

3.12	Instruments Accuracy and Uncertainty in Measurement	65
CHAPTER 4	RESULTS AND DISCUSSION	67
4.1	Introduction	67
4.2	Optimized Injection Duration	67
4.3	Validation of Numerical Analysis	69
4.3.1	Comparison of Numerical Analysis and Experimental Analysis	69
4.4	Effect of Nozzle Hole Diameter- Numerical Analysis	73
4.4.1	Numerical Investigation of the Engine Combustion Characteristics	73
4.4.1.1	In-cylinder Pressure	72
4.4.1.2	Apparent Heat Release Rate	72
4.4.2	Numerical Investigation of the Engine Emission Characteristics	75
4.4.2.1	Un-burnt Hydrocarbon Emissions	75
4.4.2.2	Carbon-monoxide Emissions	76
4.4.2.3	Nitrogen Oxide Emissions	77
4.4.3	Numerical Investigation of the Engine Spray Characteristics	77
4.4.3.1	Liquid Penetration Length	78
4.4.3.2	Break-up Length	79
4.4.3.3	Sauter Mean Diameter (SMD)	81
4.5	Summary	82
CHAPTER 5	CONCLUSION AND FUTURE WORK	83
5.1	Conclusion	83

5.2	Scope of Future Work	84
REFERENCES		86

LIST OF FIGURES

S. NO.	Title	Page No.
Figure 1.1	Stages in the Combustion Process in a Diesel Engine	6
Figure 1.2	Combustion of Lean Hydrocarbons-based Fuel with Air	8
Figure 1.3	Basic Features of a Typical DI Engine Fuel Spray	12
Figure 1.4	Schematic Representation of the Thesis Outline	23
Figure 2.1	Legislative Limit on the Emission Level of Nitrous Oxides (NO _x) and Particulates (PM) for Heavy-Duty Diesel Engine in India.	25
Figure 3.1	Flow Overview-High Level View of Simulation Task	38
Figure 3.2	Flow-Through Nozzle Passage	48
Figure 3.3	KH/RT Break-up Model for Solid Cone Sprays	50
Figure 3.4	Two-Step Approach in Implementing the KH Break-up Model	52
Figure 3.5	Computational Grid for Start of Compression Stroke	55
Figure 3.6	ECU-Nira i7r Equipped with Engine Setup	57
Figure 3.7	Eddy Current Dynamometer	58
Figure 3.8	Schematic Diagram of Common Diesel Fuel Injection System	62
Figure 3.9	Nozzle (0.26 mm Nozzle Hole Diameter) Equipped with Engine	62

Figure 4.1	Comparison-CFD Analysis and Experimental Analysis for In-cylinder Pressure and AHRR for (a) 0.20 mm NHD, (b) 0.26 mm NHD (c) 0.30 mm NHD	72
Fig 4.2	Peak In-cylinder Pressure and AHRR for 0.20 mm, 0.26 mm, and 0.30 mm Nozzle Hole Diameter-Numerical Investigation	74
Fig 4.3	Variation of Unburnt Hydrocarbon Emissions for Three Different Nozzle Hole Diameter	75
Fig 4.4	Variation of Carbon-monoxide Emissions for Three Different Nozzle Hole Diameter	76
Fig 4.5	Variation of Nitrogen Oxide Emissions for Three Different Nozzle Hole Diameter	77
Fig 4.6	Variation of Liquid Penetration Length for Three Different Nozzle Hole Diameter	78
Fig 4.7	Variation of Break-up Length for Three Different Nozzle Hole Diameter	80
Fig 4.8	Variation of Sauter Mean Diameter for Three Different Nozzle Hole Diameter	81

LIST OF TABLES

S. No.	Title	Page No.
Table 1	Values of the Model Constants	42
Table 2	CFD Sub-model	53
Table 3	Specifications of Fuel Injection System	53
Table 4	Initial and Boundary Conditions	54
Table 5	Test-Engine Specifications	56
Table 6	Parameters for Finding Optimized Injection Duration	64
Table 7	Physical Instrument Accuracy	65
Table 8	Comparison for Experimental-CFD Analysis at Optimized Injection Duration for Different Nozzle Hole Diameter	68
Table 9	Relative error for numerical-experimental (a) In-cylinder pressure and (b) AHRR at a particular crank angle degrees.	70

NOMENCLATURE

H_2O	Water
N_2	Nitrogen
O_2	Oxygen
cm^3	Cubic Centimetre
°bTDC	Degrees Before Top Dead Centre
°CA	Degree Crank Angle
AHRR/HRR	Accumulated Heat Release Rate/ Heat Release Rate
BS	Bharat Stage
BSFC	Brake Specific Fuel Consumption
BTE	Brake Thermal Efficiency
CFD	Computational Fluid Dynamics
CI	Compression Ignition
CO	Carbon Monoxide
CRDI-VCR	Common Rail Direct Injection- Variable Compression Ratio
DI	Direct Injection
ECU	Electronic Control Unit
HCCI	Homogeneous Charge Compression Ignition
IC	Internal Combustion
K	Kelvin
KW	Kilowatt
LTC	Low Temperature Combustion
MPa	Megapascal

NO _x	Nitrogen Oxides
PM	Particulate Matter
PPC	Partially Premixed Combustion
RCCI	Reactivity Controlled Compression Ignition
rev/min, rpm	Revolution Per Minute
SMD	Sauter Mean Diameter
SOI	Start of Injection
UHC	Unburn Hydrocarbons
λ	Excess Air Fuel Ratio

CHAPTER 1

INTRODUCTION

1.1 Introduction

The CI engine has been utilized by the domestic auto industry due to its thermally efficient characteristics. However, the non-homogeneous mixture of air and fuel inside the diesel engine makes its utilization less preferable as they produce extensive soot and other toxic emissions. The effective development in the diesel engine has made it controllable that has resulted in the improvement of fuel economy and effective emissions control technology. The development of effective emissions control technology due to its impact on the automotive industry was the priority of research for the past few years. Toxic pollution has been seen as a significant threat to our environment and human health. The major toxic emissions emitted from the engine exhaust are carbon monoxide (CO), unburnt hydrocarbons (UHC), nitrogen oxides (NO_x), and particulate matter (PM). This makes many countries have more stringent legal limits on the emissions of these toxic substances.

In recent years, the automotive researcher community and automobile companies have focused their research attention on enhancing the thermal efficiency of the diesel engine while lowering the toxic emissions from diesel engines. Many different methods are been utilized to improve the modern day's engine's efficiency that includes boosting intake pressure by using a turbocharger or superchargers [1], variable valve timing [2], an advanced fuel injection process in the engines [3]. In addition to this, many newer steps were taken to further enhance engine efficiency. The concepts of low-temperature combustion (LTC) i.e., HCCI, RCCI, and PPC were extensively studied [4], [5]. Although, most LTC combustion concepts cause HC and CO emissions that exceed the

legal limits because of their lower combustion temperature and the stranded of the premixed fuel in the crevices.

Automotive researchers have to utilize some other methods that can meet the emission regulations in the diesel engine without compromising its efficiency. To achieve this, researchers have focused their research on the factors that significantly influence fuel consumption, engine emissions, combustion process with the effect on the fuel-air mixture formation, spray formation, nozzle geometries, etc. One such factor is improving the process of atomization and fuel-air mixing. The recent developments in the high-pressure injection technology made it possible to achieve a fine atomization process of the fuel that significantly influenced the air-fuel mixing. Along with high-pressure injection, the variation in the geometry of the nozzle has shown the possibility to meet the emission regulations with the improvement in the combustion characteristics. To have a better insight into this, an understanding of various spray characteristics like penetration length, break-up length, and SMD is a must.

In recent times, the utilization of computational simulations in the area of engine research has been viewed as a major analytical tool. In this, they establish the correlation with the experimental studies and provide new insight to the researcher. The use of simulation tools provides the advantage of creating novel and fuel-efficient engines with lower toxic pollutants. The flexibility in the simulation steps, as well as the cost efficiencies, provides the significant boon of utilizing the simulation tools. In the present study, one such simulation tool is utilized to investigate the diesel engine characteristics. In the present market, the main commercial CFD software available are ANSYS-Forte & -Fluent, AVL-FIRE, along STAR-CD and STAR-CCM+.

In addition to these, open-source code-KIVA and OpenFOAM are also becoming more popular. ANSYS-Forte CFD package has been chosen for the present study to utilize its benefits of automatic mesh generation with better time efficiency. The Chemkin-pro solver in the package provides the computational speed required for the simulation of the predictive engine. The presence of multi-components fuel-vaporization models allows the effective prediction of fuel sprays effects as well as representation of the physical spray. ANSYS Forte enables the reduction in dependency of grid and time-step due to the presence of advanced spray models.

1.2 Combustion in CI engine

Combustion refers to a chemically oxidized exothermic gas-phase reaction process in which the fuel and oxidant get combusted to generate heat and/or work. The combustion process in the diesel engine effectively controls engine power, efficiency, and emissions [6], [7]. The process of combustion includes the injection of fuel into the combustion chamber through the injector nozzle. The fuel injection is done at high pressure and high velocity through the nozzle orifice present at the injector tip end. The formation of a single or multiple jets occurs during the injection that depends upon the nozzle geometry. After the fuel passed the injector tip, it gets atomized into smaller droplets that penetrate into the combustion chamber. The smaller fuel droplets vaporize and mixed with the high-temperature air. This resulted in the spontaneous burning of some premixed air-fuel mixture after the ignition delay which is characterized as the start of combustion. A sharp rise in the cylinder pressure is observed as the premixed air-fuel mixture burns. The burning of the premixed air-fuel mixture increases the pressure inside the combustion chamber that tends to compress and burns the remaining portion of the air-fuel mixture.

This causes a reduction in the ignition delay period. The combustion inside the cylinder continues until all the injected fuel gets atomized, vaporized, and mixed with air has combusted. The combustion process inside the cylinder is unsteady, 3-Dimensional, and heterogeneous in nature. Also, the combustion process inside the engine cylinder depends on the fuel characteristics, injection system and combustion chamber design, and operating conditions of the engine.

The process of combustion takes place in three stages in a diesel engine;

First Stage: This stage includes a very high rate of burning that remains for only a few crank angle degrees and is characterized by the rapid rise in pressure inside the cylinder.

Second Stage: This stage includes the gradual reduction in the heat release rate before it initially rises. It is marked as the period of the main heat release and lasts for major crank angle degrees. During the first two stages, almost the entire energy is released from the fuel.

Third Stage: This includes the small and distinct heat release rate which continues throughout the expansion stroke. It is marked as the tail of the heat-release curve. A small heat release is observed during this stage from the fuel.

During the combustion process, the following characteristics can be observed.

- The fuel injection period is lesser than the total burning period of the air-fuel mixture.
- The speed of the engine defines the burning rate which is proportional to the engine speed. This ensures the constant burning interval on a basis of crank angle.

- The ignition delay period influences the magnitude of peak burning rate which is higher due to long delays.

The overall combustion process of the air-fuel mixture in the diesel engine is shown in Figure 1.1 and can be defined under the following periods,

Ignition Delay (ID) period: ID is the period between the SOI and SOC. It is marked on the pressure-crank angle diagram with the variation in slope.

Pre-mixed combustion period: It is the period of the rapid burning of the air-fuel mixture mixed during the ignition delay period. The burnt product is later mixed with the injected fuel for combustion. This period is marked by the high heat-release rate.

Rate-controlled combustion period: After the combustion of the premixed air-fuel mixture is completed during the ignition delay period, the combustion process depends on the rate at which the air-fuel mixtures are available for combustion. During this period, the atomization and vaporization of the injected fuel are controlled which later form the air-fuel mixture by mixing with the air. This resulted in the controlled pre-flame chemical reactions and fuel-air mixture burning rate. The rate of heat release is relatively lower than the premixed combustion period which decreases further as the period progresses.

Late combustion period: During this period, the rate of heat release continues, however at a relatively lower rate during the expansion stroke. This is due to the small amount of heat released from the soot and products in a fuel-rich combustion zone. The mixing of non-uniform air-fuel mixture encourages the complete combustion of the mixture and thus causes less dissociated product gases.

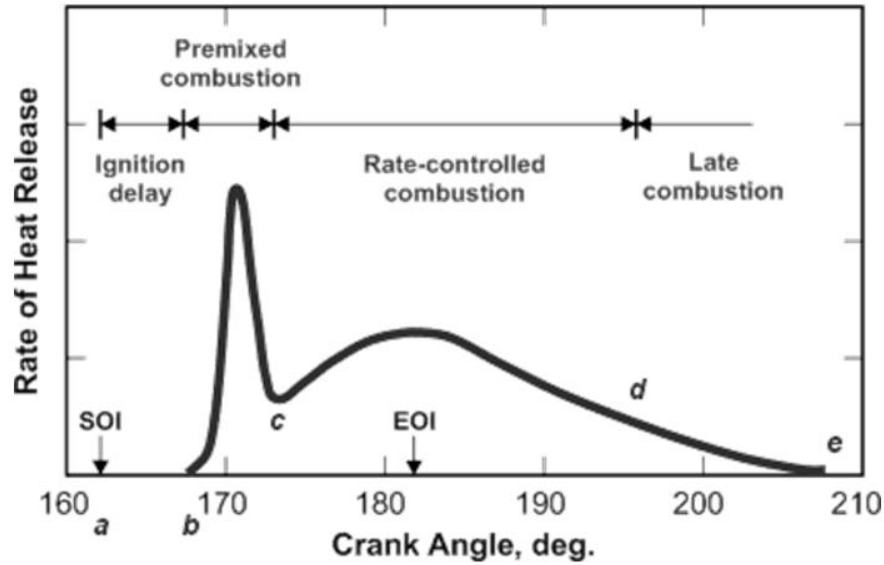


Figure 1.1. Stages in the combustion process in a diesel engine [8].

1.3 Emissions in CI engine

The complete combustion of hydrocarbon-based fuel ($C_\alpha H_\beta O_\gamma$) and air leads to the formation of CO , O_2 , N_2 , and H_2O as shown in Figure 1.2. The formation of O_2 occurs only if there exists a lean mixture. The excess air-fuel ratio (λ) is given by the ratio of actual air-fuel ratio to the stoichiometric air-fuel ratio. It measures the deviation of the actual air-fuel mixture from the stoichiometric mass ratio [9]. The excess air-fuel ratio is given by:

$$\lambda = \frac{\text{Air mass}}{\text{Fuel mass} * \text{Stoichiometric ratio}} \quad (1.1)$$

where

- $\lambda > 1$ is for the lean mixture,
- $\lambda < 1$ is for the rich mixture,
- and, $\lambda = 1$ is for the stoichiometric mixture.

The reciprocal of λ is known as the equivalence fuel-air ratio, represented by ϕ , can also be used. Although, the complete combustion of hydrocarbon-based fuel ($C_\alpha H_\beta O_\gamma$) and air yields non-toxic products, but the formation of CO_2 is a concern as it is known as a greenhouse gas and causes global warming. On the other hand, combustion in the case of practical applications always causes toxic species like HC, CO, PM, and NOx because of incomplete combustion. The major combustion pollutant species are listed below with their effect on the local environment:

1.3.1 Un-burnt Hydrocarbons (UHC)

HCs in diesel exhaust include either decomposed fuel molecules or recombined intermediate compounds [10]. These exhibit in different forms that contain paraffin, olefin, and aromatic hydrocarbons $C_m H_n$. The formation of aldehydes ($C_n H_m CHO$), ketones ($C_n H_m CO$), and carboxylic acids ($C_n H_m COOH$) is due to the partial combustion of hydrocarbons [11]. Another source for HC formation in diesel exhaust is lubricating oil. HCs sources in a diesel engine are mainly due to over-mixing or under-mixing of air and large size fuel droplets during the end of injection. Generally, the HCs formations depend on lean-flame-out-region (LFOR), part of fuel injected on the cylinder wall, spray cone and tail, and after injection techniques. Engine design and operating conditions also influences the oxidation and formation of HCs.

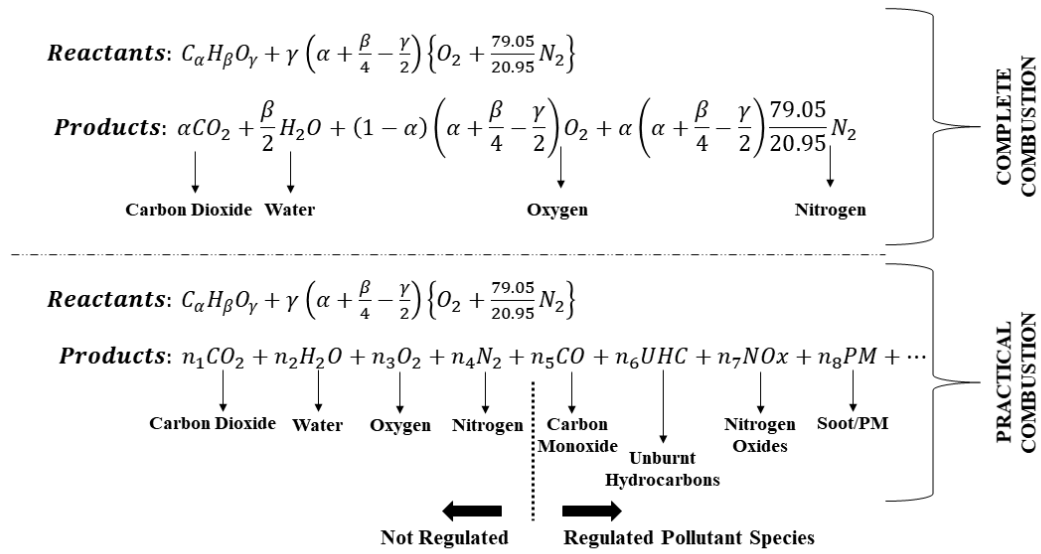
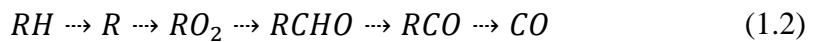


Figure 1.2. Combustion process of hydrocarbon-based fuel and air [11].

1.3.2 Carbon monoxides (CO)

CO emissions are tasteless, colorless, and odorless toxic gas that has the capability of harming or even killing humans by reacting with the oxygen in the bloodstream. It is marked as the intermediate product formed during the combustion of hydrocarbons [12]. In the combustion mechanism of hydrocarbons, the formation of CO is considered one of the important reaction steps. The hydrocarbons breakdown process is shown in Equation 1.2 in which the hydrocarbon radical is represented by R [8].



The lack of oxidants, temperature, and residence time resulted in CO formations due to partial combustion. However, for complete combustion, CO oxidizes into the CO_2 because of the recombination reactions occurring between CO and different oxidants (Equation 1.3). The only time CO will be left un-oxidized is when there occur incomplete reactions due to lower air temperature or lack of oxidants [13]. The rich-fuel mixtures combustion usually causes high CO formation but leaner diesel

combustion and rich air quantity cause lower emissions of CO from diesel combustion. During the different periods of combustion inside the diesel engines, the conditions that promote CO oxidation are:

- Low air-fuel ratio,
- High oxygen content,
- High combustion temperature, and
- High air-fuel mixing rate.

1.3.3 Nitrogen Oxides (NO_x)

The NO_x emissions take into consideration both nitric oxide (NO) and nitrogen dioxide (NO₂) in the exhaust of a diesel engine. In DI diesel engines, NO includes 70% to 90% of the total NO_x. NO is considered as the combustion by-product instead of CO which is a compound in transition. The intake air charge comprises more than 75% nitrogen by volume. The balanced oxygen in the entrained air and the combustion of hydrocarbon fuel ensure the continuation of the NO_x formation until it has exhausted from the engine tailpipe. The fuel-NO_x concentration is negligible and therefore its contribution to the chemical reactions is neglected.

The NO formation is characterized by the extended Zeldovich mechanism given by Equations 4 to 6:



When the O₂ molecule comes in contact with a high-temperature N₂ environment, the formation of NO takes place with a residual of a single N atom formed in an unstable and energetic state (Equation 1.4). The N atom reacts with O₂ (present inside the

cylinder) in the presence of heat available from the combustion process and attains a stable state. This consequently leads to the higher formation of nitric oxides while leaving the oxygen atom in an unstable state (Equation 1.5). In the Zeldovich mechanism, the formation of radical OH^* takes place that forms more NO and H atoms after reacting with the N atoms (Equation 1.6).

Overall, the three equations show the mechanism by which NO can be formed, and the longer the residence time in this high NO formation regime, the larger are the NO_x concentrations. According to the Zeldovich mechanism, the chain reaction does not initiate by the N atom because of its lower concentration against the concentration of oxygen during the combustion process [14]. Therefore, the local temperature influences the formation of NO in the spray during the combustion process. The reaction of NO with excess oxygen causes the NO_2 formation. However, the cylinder wall-quenching due to excess air can result in the restriction of NO formation. During the expansion stroke, as the temperature tends to decrease, the concentration of NO does not reduce to the limit concentration because the NO attains stability under these conditions. From the previous studies [15], [16] it was shown that the NO removal process during the expansion stroke is slow which makes the NO concentration to be constant for the entire expansion stroke. This phenomenon occurs mainly in the lean fuel-air mixtures [17]. The premixed portion of the fuel burned before the system has achieved maximum cylinder pressure contributes to the main reason for NO formation.

With the termination of the combustion process, the NO is compressed to elevated pressure and temperature. That's why NO_x control techniques focus mainly on the early phase of combustion. However, the effort of reducing the combustion temperature leads to penalties in the formation of HCs, PM with higher fuel consumption. Thus, it is required to make NO_x/PM trade-off or $NO_x/fuel\ consumption$ trade-off in the diesel

engines. [18] has found that the factors that affects the initial heat release rate will also influence the NO_x formation rate in the same manner. Therefore, many control techniques are attempted to minimize the fuel burnt quantity during the premixed burning period that includes initial rate shaping using a lower injection rate during the injection period followed by a substantially higher injection rate after the combustion initiates. The technique also includes pilot injection, which has a separate small injection to start the combustion with minimum fuel quantity that is followed up by the main injection after the combustion has started.

1.4 Diesel Spray Fundamentals

The injection of liquid fuel into a CI engine is achieved through single or multi-nozzle orifices having a larger pressure difference between the cylinder and fuel delivery line. Depending on the needs and size of the combustion system, the design of the nozzle can either be single/multi-hole or throttle/pintle. Figure 1.3 portrays the basic features of fuel spray in a diesel engine. After exiting the nozzle tip, the fuel jet atomizes into fine droplets whose momentum creates a spray and spreads out as the spray enters the surrounding air. [19] has found that the initial jet velocity of fuel spray is very high. The disintegration of the liquid surface into the smaller droplets occurs as the liquid jet passes the nozzle exit.

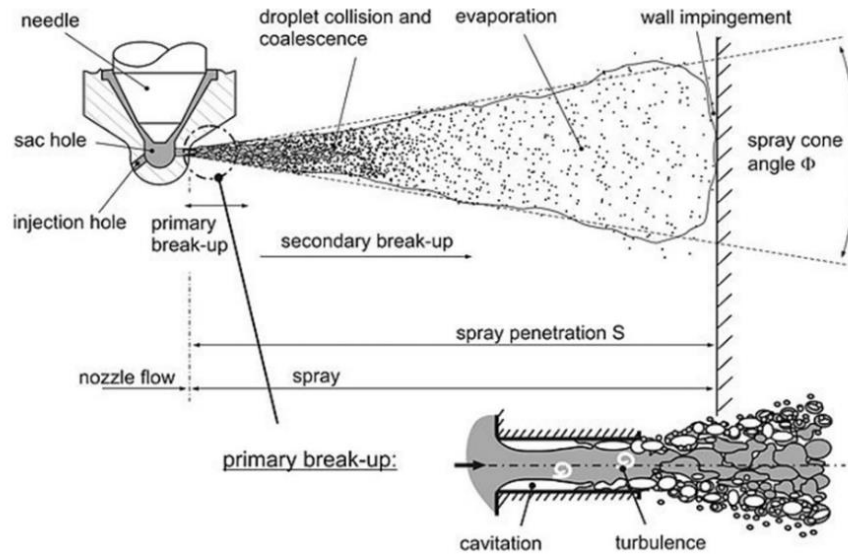


Figure 1.3 Basic features of a typical DI engine fuel spray [20].

With the forward motion of the injected fuel from the nozzle, the concentration of air mixed with the fuel spray increased that diverges the fuel spray increased its width, however, the velocity has decreased. As this hot air proceeds, fuel drops get evaporated. With the continuation of injection of fuel, the spray tip gets penetrated further into the combustion chamber. However, the rate of penetration keeps on decreasing. After the fuel spray penetrated the outer region, it has contacted the cylinder wall that causes the spray to split and then flows in a tangential direction along the wall. The liquid droplets and ligaments accumulate near the nozzle with the maximum region of spray include of fuel vapor and the air around the narrow core that contains remaining liquid fuel. Near the nozzle, the ligaments and liquid droplets occupy the major region consisting of air-clouds and fuel vapors around the confined core where the remaining liquid fuel is accumulated. Within this region, the autoignition occurs which raises the mixture temperature at the time of the “premixed combustion period”. This then leads to the “rate-controlled combustion” period of the diesel combustion process in which the lifted off diffusion flames surrounded the liquid spray near the end of the injector

nozzle. Most of the combustion systems use air swirls to increase mixing rates of fuel and air. The swirl enhances the radial as well as tangential motion of spray that causes the formation of a more complex structure of the liquid jet [21]. After the mixing of air with fuel spray, it gets slower and curves towards the direction of swirl. There observed less penetration of spray with the swirl than without it, while keeping similar injection conditions. The significant function of spray is to form a region of large vapor below the core that contains the liquid fuel.

1.4.1 Atomization and Spray Development

The process of atomization involves the breaking up of bulk liquid into smaller droplets due to the disruption in the surface tension force of the liquid by the internal and external forces. The surface tension force causes the liquid fuel to form a sphere because of its minimum surface energy. However, the presence of aerodynamic forces on the liquid surface disrupts this surface tension due to the effect of external force on the mass of liquid. With further increases in the external forces, the breaking up of bulk liquid takes place. During the initial atomization process, many unstable large droplets are formed that further undergo the breaking up process to form relatively small droplets. Therefore, the final size of the droplets formed depends on [22]-

- *Primary breakup*: Droplet size formed during the primary atomization
- *The secondary breakup*: The extent to which droplets formed during the primary breakup is further disintegrated.

However, the rate of droplet disintegration depends on either its steady acceleration or sudden exposure to a gas stream at high velocity.

When the fuel has injected into the engine cylinder, it rapidly breaks up into smaller droplets forming a cone-shaped spray. This behavior comes under the atomization breakup regime (or first wind-induced break-up regime) in which the droplets formed to have a smaller diameter compared to the diameter of the nozzle exit. While in the Rayleigh regime (or second wind-brak-up regime), the higher jet velocity further disintegrated the liquid jet. This occurs because of the unstable surface waves formed due to the surface tension that causes smaller droplets size than the nozzle diameter. As the jet velocity reaches the maximum, it causes the formation of an atomization region in which the break-up of the spray peripheral surface occurs. This resulted in the size of the droplets minimum at the exit of the nozzle plane. The presence of aerodynamic forces on the fuel-air interface is one of the important characteristics of the atomization regime mechanism [23].

1.4.2 Spray Penetration

It is defined as the velocity and distance upto which the penetration of the fuel spray into the combustion chamber occurs. [24] found that the spray penetration influences the air-utilization and its mixing with the fuel. Although, in some applications (presence of a swirl), the impingement of fuel is required on the cylinder wall where the wall is at a higher temperature. However, in multiple injections system, over-penetration of fuel makes the liquid fuel impinges on the cool wall which having swirl or no swirl, causes the reduction in mixing rate of the fuel-air mixture. This results in higher emission of HC with the combination of partially burned species. Also, the under-penetration of the fuel can cause poor utilization of air since the air near the wall will not get in contact with the sprayed fuel [25]. Therefore, there has been an extensive

study on the penetration of liquid fuel spray under conditions similar to that found in diesel engines.

For this, several empirical relationships have been proposed for spray penetration of fuel using the experimental data and turbulent gas jet theory. These relationships help in predicting the spray tip penetration with respect to time across the combustion chamber. More recent work has compared vaporizing sprays with non-vaporizing sprays. For short time and penetrations, and long time and penetrations, the difference in jet penetration is small. In between, the differences are more significant. Also, the higher injection pressures lead to faster penetration due to the higher initial liquid-fuel momentum.

A scaling law for non-vaporizing spray penetration developed by [26], expressed in the dimensionless form:

$$\tilde{t} = \frac{\tilde{S}}{2} + \frac{\tilde{S}}{4} \sqrt{1 + 16\tilde{S}^2} + \frac{1}{16} \ln \left(4\tilde{S} + \sqrt{1 + 16\tilde{S}^2} \right) \quad (1.7)$$

where the dimensionless time and penetration length are given by:

$$\tilde{t} = t/t^+ \text{ and } \tilde{S} = S/x^+ \quad (1.8)$$

t^+ and x^+ represents the characteristics of fuel spray time and length scales and are defined by:

$$t^+ = \frac{d_n \sqrt{\tilde{\rho}}}{\tan\left(\frac{\alpha}{2}\right) U_f} \text{ and } x^+ = \frac{d_n \sqrt{\tilde{\rho}}}{\tan\left(\frac{\alpha}{2}\right)} \quad (1.9)$$

The orifice diameter (d_n), density ratio ($\tilde{\rho}$), and fuel velocity (U_f) are related as:

$$d_n = \sqrt{C_a d}, \tilde{\rho} = \frac{\rho_f}{\rho_a}, \quad (1.10)$$

and

$$U_f = C_v \sqrt{2(P_f - P_a)/\rho_f} \quad (1.11)$$

where C_a and C_v represents the orifice area concentration coefficient and velocity coefficient, respectively, and P_f and P_a represents fuel injection pressure and local air pressure.

The penetration distance \tilde{S} as a function of time is given by:

$$\tilde{S} = \tilde{t}/(1 + t^{-n/2})^{1/n} \quad (1.12)$$

In medium and light-duty DI diesel engines, fuel-air mixing is achieved by utilizing the air swirl [21]. As the size of the cylinder decreases and maximum engine speed increases, a higher swirl is created and enhanced during intake as the in-cylinder air is forced radially inward towards the cylinder axis during compression with reduced bowl diameter/bore ratios and deeper bowls. The air swirl significantly affects the spray penetration [27].

1.4.3 Sauter Mean Diameter (SMD)

In addition to the fuel injection process, the atomization of that fuel into smaller droplets is also necessary, which have a high velocity. This is required to achieve a larger surface area of droplets across which the evaporation of liquid fuel can take place. The measurement of droplet sizes is difficult during the running of diesel engines. However, [28], [29] have carried out an investigation using the constant-volume chamber in which the high-pressure stationary air is present at room temperature. Then the injected fuel is mixed with this high-pressure-air present in the chamber. [30] has shown that the

distribution of droplets size at a given location in the spray can be influenced by varying different injection conditions during the injection period. Also, the path of individual droplets gets affected by their size, location, and velocity.

The jet breakup process in the atomization regime is combined with the G.I. Taylor work to predict the initial average droplet diameter D_d . The droplet diameter proposed by their work is given by:

$$D_d = C \frac{2\pi\sigma}{\rho_g v_r^2} \lambda^* \quad (1.13)$$

Here, σ represents the liquid-fuel surface tension, ρ_g represents the gas dynamic, v_r represents the relative speed between liquid and gas (mean injection velocity), C represents unit order constant, and λ^* is a dimensionless quantity given by $(\rho_l/\rho_g)(Re_j/We_j)$.

Equation (1.13) predicts the trends observed for droplet size at the edge of the spray with respect to different injection parameters. However, during initial spray formation, coalescence and breakup phenomenon for the droplets causes the variation in the size distribution and its diameter. The size of droplets in the conical sprays is influenced by the secondary atomization phenomenon. Finally, a balanced is reached during the expansion of the spray due to the decrease in the coalescence. This terminates the breakup process because of the low relative velocity between the droplet and air.

Distribution of droplets size is usually expressed as the frequency distribution of droplet volume. If $f(D_d)dD_d$ is the probability of finding a droplet with a diameter D_d and $D_d + dD_d$, then

$$\int_0^{\infty} d(D_d) dD_d = 1 \quad (1.14)$$

and the volume distribution is:

$$\frac{1}{V} \frac{dV}{dD_d} = \frac{f(D_d)D_d^3}{\int_0^{\infty} f(D_d)D_d^3 dD_d} \quad (1.15)$$

With the away movement of spray from the nozzle orifice, there is an increase in the average droplet size that occurs because of some droplet coalescence and vaporization into the smaller droplets in the distribution. The average droplet size decreases as we move radially outward from the spray axis, presumably due to higher local concentrations of hotter entrained air, and higher droplet evaporation rates.

The relationship between the droplets mean diameter and size distribution is given by the sauter mean diameter as:

$$D_{SM} = \left(\int D_d^3 dn \right) / \left(\int D_d^2 dn \right) \quad (1.16)$$

where dn represent the droplets numbers having a diameter D_d between $D_d - dD_d/2$ and $D_d + dD_d/2$. The integration is performed for an appropriate number of droplet sizes. The SMD of the droplets can also be described as the diameter having the identical surface/to volume ratio as compared to total droplet distribution.

Various relationships have been proposed for the droplet size distribution within the liquid sprays have been proposed. [31] in his work have proposed an expression based on the chi-square statistical distribution that fits the available experimental data.

The non-dimensional expression is given by:

$$\frac{dV}{V} = 13.5 \left(\frac{D_d}{D_{SM}} \right)^3 \exp \left[-3 \left(\frac{D_d}{D_{SM}} \right) \right] d \left(\frac{D_d}{D_{SM}} \right) \quad (1.17)$$

[31] has also proposed an empirical relationship for the SMD (D_{SM}) which is given as:

$$D_{SM} = A(\Delta p)^{-0.135} \rho_a^{0.121} V_f^{0.131} \quad (1.18)$$

where Δp represents the drop of pressure across the nozzle (in MPa), ρ_a represents the air-density (in kg/m^3), and V_f represents the fuel delivery rate per cylinder (in $\text{mm}^3/\text{stroke}$). The constant "A" depends on different nozzles types whose values are given by:

- Throttling pintle nozzle – 22.4
- Hole nozzle – 23.9
- Pintle nozzle – 25.1

[32] have observed that the SMD gets affected by the injection pressure, nozzle geometries, and entrained fuel and air properties. [33] also have observed similar results for the nozzle L/D ratio. [34] have found that the fuel viscosity and surface tension affects the mean droplet-size at lower injection pressures.

1.4.4 Spray Evaporation

As discussed earlier, after the fuel is injected into the cylinder, it atomizes to form smaller droplets. This is followed by the formation of spray that vaporizes before mixing with the air and the combustion process takes place. There exist a core along the axis of the spray where the liquid fuel ligaments or drops are sufficiently dense. As the initial injection phase is completed, the core-length containing the liquid fuel remains constant till the injection ends. The large vapor-containing spray region

surrounds the liquid core. However, the vapor region penetrates further away with respect to the core that penetrates partially to the tip of the spray. According to [25], the droplet evaporation process is relatively quick with respect to the total combustion periods under normal engine operating conditions.

The application of energy balance in combination with the spray mass and momentum balance for the one-dimensional evaporating spray model gives the scaling law for liquid fuel penetration. During the maximum penetration of the liquid core, enough energy is transmitted to the liquid drops from the hot entrained air that fully vaporizes the fuel. It is also assumed that at the liquid length, saturated fuel vapor conditions pertain and that air entrainment rates for the vaporizing spray differ little from those of a non-vaporizing spray. That is, the spray penetration length scaling law and its inverse defines the overall spray behavior [35]. The liquid scaling law in the dimensionless form is derived as:

$$\tilde{L} = 0.47 \sqrt{\left(\frac{2}{B(T_a, p_a, T_f)} + 1\right)^2 - 1} \quad (1.19)$$

where, $\tilde{L} = L_t/x^+$ with x^+ defined by equation

$$x^+ = \frac{d_n \sqrt{\tilde{\rho}}}{\tan\left(\frac{\alpha}{2}\right)} \quad (1.20)$$

and,

$$\begin{aligned}
B(T_a, p_a, T_f) &= \frac{Z_a(T_s, p_a - p_s)p_s M_f}{Z_f(T_s, p_s)(p_a - p_s)M_a} & (1.21) \\
&= \frac{h_a(T_a - p_a) - h_a(T_s, p_a - p_s)}{h_f(T_s) - h_f(T_f, p_a)}
\end{aligned}$$

The energy balance on the fuel spray in combination with the equation of states gives equation (1.21) in which expressions are for single-component fuels. In this equation, T_s represents the fuel-air mixture temperature, T_a represents ambient air temperature, p_a & p_s represents the ambient air pressure and fuel partial pressure at the given liquid length. The variables h_a and h_f represents air and fuel-specific enthalpies, and M_a and M_f represents air and fuel-molecular weight, and Z_a and Z_f represents the compressibilities of the fuel vapor and air at saturated conditions.

1.5 Thesis Organization

The thesis entitled “**Some studies on engine combustion, emission, and spray characteristics of a CRDI diesel engine with variable nozzle geometry using ANSYS**” is divided into five chapters, and is outlined as:

Chapter 1 introduces the reader to the research conducted in the area of internal combustion engines. It shows how automotive researchers have shifted their area of focus toward enhancing the CI engine thermal efficiency and reducing toxic emissions. The significance of diesel spray fundamentals is then discussed in the chapter. Varying the nozzle geometry has shown promising results in this. Hence one such nozzle geometry has been varied to investigate its effect on the diesel engine characteristics. ANSYS-Forte CFD package has been chosen for performing the present research work.

In the second chapter, the existing literature is critically reviewed. The chapter consisted of three sub-components. In the first, the effect of variation in the nozzle geometry on combustion and performance characteristics is discussed. Later, the effect of variation in the nozzle geometry on emission characteristics is discussed. Finally, the effect of variation in the nozzle geometry on spray characteristics is discussed. The chapter also includes the summary from the literature review discussed.

In the third chapter, the different models included in the ANSYS-Forte CFD package are discussed. Then, the simulation setup with the boundary conditions for the diesel engine is discussed. Finally, the development of the engine test setup and the test procedure is described. The uncertainty and accuracy involved in this study are also reported.

In the fourth chapter, the outcomes of the numerical investigation on the engine characteristics are discussed in detail and the findings are compared with the existing literature. The validation of the numerical analysis with the experimental data is also discussed in the chapter. Lastly, in the fifth chapter, the major outcomes from the present research are outlined and the future recommendations are provided.

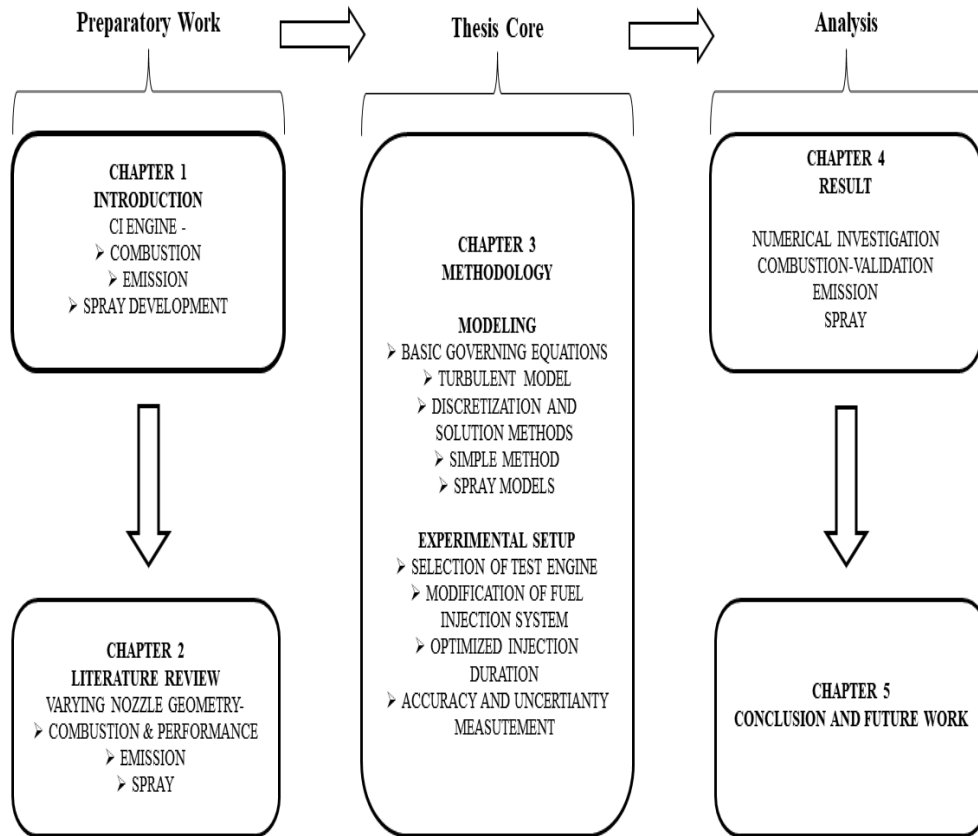


Figure 1.4 Schematic representation of the thesis outline.

CHAPTER 2

LITERATUR REVIEW

2.1 Introduction

The research developed in the field of CI engines has been at its peak in recent times. The advancement in new technologies within the engine has elevated the demand for new engine types. Further, the environmental constraints on the engines have become strict over years. Figure 2.1 shows the legislated limit on the emission levels of nitrogen oxides (NO_x) as well as particulates (PM) for heavy-duty diesel engines in India. Other species like unburned hydrocarbons and carbon monoxide are also regulated. The automotive researcher community and automobile companies have focused their research attention on improving the engine's efficiency while minimizing the pollutant emissions from CI engines. Many different methods are used to improve the modern day's engine's efficiency that includes boosting intake pressure by using a turbocharger or supercharger [1], variable valve timing [2], an advanced fuel injection process in the engines [3]. In addition to this, many newer steps were taken to further enhance engine efficiency. The concepts of low-temperature combustion (LTC) i.e., HCCI, RCCI, and PPC were extensively studied by [4], [5]. The results showed improved indicated BTE with lower NO_x emission and soot. Apart from this, a very large amount of literature on engine research is available. In this section, the literature review related to the present study has been presented.

The fuel injection system has greatly influenced the combustion phenomenon in diesel engines. As the combustion process is heterogeneous in nature, controlling it significantly improves efficiency and emissions formation [6], [7]. Thus, a better understanding of the in-cylinder combustion, emission, and spray characteristics may

further improve the engine efficiency with the control over fuel economy and emission formations. To achieve this, various experimental-CFD works have been done in the past. A major review of the available literature on nozzle geometry is presented in the following section.

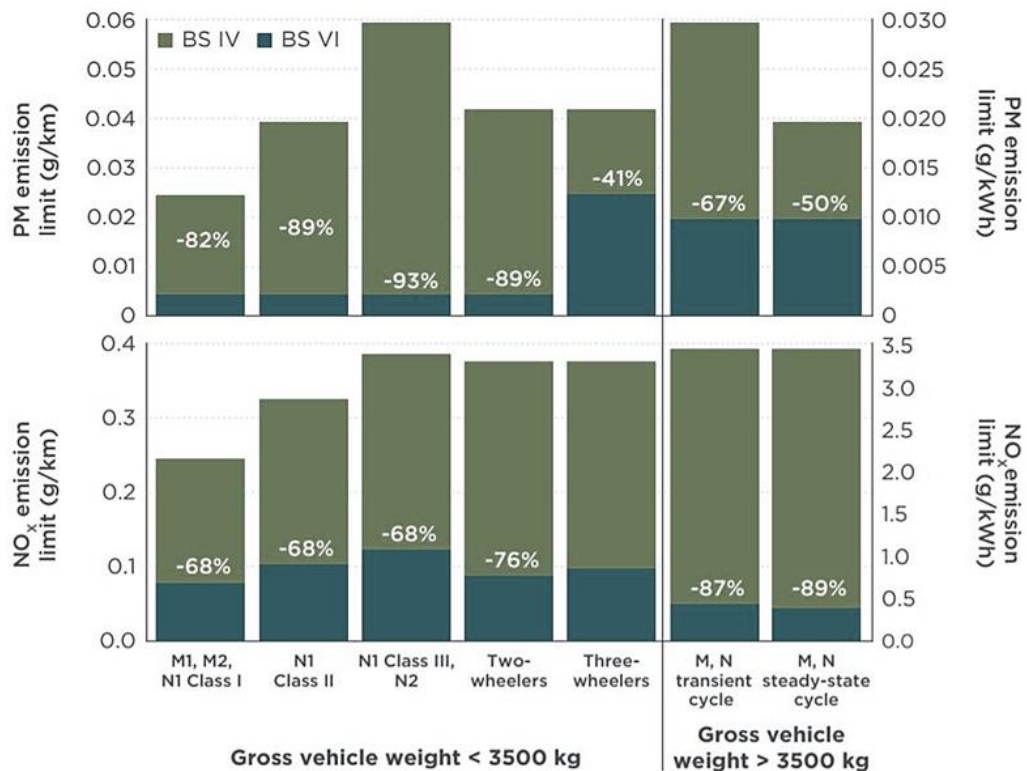


Figure 2.1. Legislated limit on the emission levels of nitrogen oxides (NOx) as well as the particulates (PM) for heavy-duty diesel engines in India [36].

2.2 Combustion and Performance Characteristics with Varying Nozzle Geometry

As stated above, the combustion process significantly improves the engine's efficiency and emission formations. Therefore, various numerical and experimental studies have been performed to enhance the combustion process inside the cylinder. In the subsequent section, the studies performed by various researchers on different nozzle geometry are studied.

[37] studied the effect of varying injector hole numbers (7 to 10) upon the performance and emission characteristics for a light-duty diesel engine running under different conditions. The author has observed improvement of ISFC-NO_x and Soot-NO_x trade-offs for lower hole diameter. Also, PM has reduced effectively with an increase in hole numbers. For low load conditions with 10- hole injector; the cylinder pressure and AHRR were higher against a 9-hole injector. For medium and high loads, the cylinder pressure and AHRR were lower for a 9-hole injector with higher PM emissions.

[38] has investigated the effect of nozzle hole geometry in a diesel engine fuelled with kapok biodiesel. In this study, the holes are varied from three to five. For higher blends, the peak HRR and in-cylinder pressure increased by 32.5% and 10% for 5 holes at full load conditions. Also, a shorter ignition delay duration was observed for 5 holes nozzle with an increase in the BTE by 6.1%.

[39] has analyzed the effect of fuel injection pressure (188 bar to 224 bar) and injector nozzle holes (3 to 5) in a diesel engine fuelled with preheated palm oil methyl esters inside the diesel engine. The fuel injection timing varied from 19, 23, and 27 °bTDC. The result showed improvement in BSFC and BTE, while a reduction in CO and HC emissions, for increasing pressure to 212 bar, with four-hole nozzle, and injection timing of 27 °bTDC.

[40] conducted an experimental study for investigating the effect of a number of holes in the nozzle on combustion and emission characteristics of dual-fuel engines fuelled with ethanol/diesel. The study includes the injectors having 4, 5, 6, and 8 nozzle holes. The result showed a reduction in peak pressure rise rate with the reduction in nozzle holes. Also, with the reduction in nozzle holes, the NO_x emission decreased while the soot, UHC, and CO emissions increased slightly.

[41] has investigated the effect of the geometry of nozzle and combustion chamber on the performance of a diesel engine fuelled with Honge Methyl Ester and producer gas. The study consists of 3, 4, and 5 nozzle holes, 0.20, 0.25, and 0.30 mm hole diameter, and varying injection pressure from 210 to 240 bar. Also, the hemispherical and re-entrant-type combustion chambers have been utilized in the study. The result indicated maximum performance for 4 holes, 0.25 mm hole diameter, 230 bar injection pressure, and re-entrant type combustion chamber. There is a 4-5% increment in BTE with a reduction in emission levels.

[42] has experimentally analyzed the effects of modified nozzle geometry on the diesel engine fuelled with a blend of Calophyllum inophyllum biodiesel and diesel, and the addition of cerium oxide nanoparticles. The experiment involved three injector nozzles with different holes and diameters (3 holes and 0.280mm, 4 holes and 0.220mm, 5 holes and 0.240mm). The findings are improvement in BTE, BSFC, and smoke levels for 5 holes nozzle compared to 3 holes nozzle.

[43] has conducted an experimental study to investigate the performance of diesel engines fuelled with cottonseed oil methyl esters for different injection timing, injector opening pressure, and nozzle geometry. The analysis involved varied fuel injection timing from 19 to 27 °bTDC; varied injection pressure from 210 to 240 bar, and nozzle holes from 3,4, and 5, each having 0.3mm in size. The result shows an overall increase in the BTE while a decrease in HC, CO, and smoke emissions for operating conditions having 19 °bTDC injection timing, 230 bar injection pressure, and 0.3mm nozzle diameter with 4-holes.

[44] has studied the nozzle hole number effect on the performance and emissions of a diesel engine fuelled with blends of diesel and biodiesel. The experiment includes

injector hole size (in μm) and the number of 340X2, 240X4, 200X6, and 170X8. The findings are a reduction of BSFC with an increase in nozzle hole number.

[45] has investigated the effect of modified nozzle geometry in DI diesel engine fuelled with blends of Calophyllum Inophyllum Methyl Esters and cerium oxides nanoparticles. The investigation includes three injectors with: base- 3 holes and 0.280mm dia, modified- 4 holes and 0.220 mm dia, and 5 holes and 0.240mm dia. The result shows that improvement in BTE and reduction in BSFC and emissions levels for 5 holes and 0.240mm diameter injector nozzle compared to 3 holes and 0.280mm diameter injector nozzle having nozzle opening pressure of 250 bar.

[46] has conducted emission and performance study using a constant volume cold spray chamber for varying nozzle hole numbers and their sizes. The study includes an injector nozzle of 225X8, 260X6, 260X8, and 300X6. The result shows that the second-best performance characteristics were found for the smallest hole size nozzle having the fewest hole numbers.

2.3 Emission Characteristics with Varting Nozzle Geometry

[47] has investigated the effect of nozzle geometry, injection timing, and injection pressure on a diesel engine fuelled with the vetia-peruviana methyl esters. The authors found that 230 bar injection pressure, 26 °bTDC injection timing, and 5-hole nozzle increased the BTE and NO_x emissions while reducing the HC, CO, and smoke emissions.

[48] has studied the effect of injection parameters on the performance and emission characteristics of a diesel engine fuelled with a diesel-producer gas blend. The study has injector nozzles with diameters of 0.2, and 0.25, and 0.3 mm with 4, 5, and 6 holes. The authors have found 4.5% higher BTE with a 4-hole nozzle for the diesel-producer

gas operation. Also, a decrease in the emission levels of 15-30% was observed for the HOME-producer gas having 240 bar injection pressure and 0.25 mm nozzle diameter with 6 holes than those of other geometries.

[49] has conducted a study to investigate the emission characteristics in a diesel engine for various operating conditions running on diesel-spirulina microalgae-ethanol blends. The study includes varying fuel injection timings (15.5 ° bTDC- 27.5 °bTDC), nozzle diameter (0.15 mm-0.4 mm), and swirl ratios (0.5-3.0). The result obtained showed increasing the nozzle hole diameter, injection timing, and swirl ratio increased the NOx emissions. However, nozzle diameter of 0.25 mm with spirulina microalgae and ethanol-blended fuel showed a better response.

[38] has conducted an experimental analysis of a diesel engine for different nozzle hole geometry fuelled with kapok biodiesel. The study includes the variation of holes number from 3 to 5. The experimental result has shown a decrease in HC, CO, and smoke emissions and an increase in NOx emission with an increase in the number of holes. Also, the BTE was found to be increased for the 5-holes nozzle against the 3-holes nozzle at full load conditions.

[50] had experimentally studied the effect of modified inlet valve and injector nozzle geometry on a TDI dual-fuel engine running with blends of calophyllum-diesel and waste wood chip gas. The study showed that the smoke opacity and nitric oxide for IVM-90 were reduced respectively by 42.7% and 48.1% and for the 4-hole nozzle were reduced respectively by 32.4% and 41.7% with a marginal increase in CO and HC for IVM-90 by 16.6% and 4.5% while for 4-hole nozzle by 16.7% and 6.7%.

[51] has investigated the performance and emission characteristics combined of the effect of the geometries of the combustion chamber and injector nozzle in a diesel

engine fuelled with POME biodiesel. The experiment involved baseline shape (HCC shape with 3 nozzle holes) and modified shapes (CCC, SCC, and TCC with 5 nozzle holes) for the combustion chamber. The author has found a decrease in CO emissions for modified-CCC and baseline-HCC shapes as compared to modified-SCC & TCC shapes at full load conditions.

[52] has experimentally performed a study on the combustion and emission characteristics for the different nozzle-hole numbers in a dual-fuel engine fuelled with ethanol-diesel blends. The investigation involves four injectors having 4, 5, 6, and 8 holes. The author found that NO_x emission decreased with a reduction in nozzle holes while the soot emissions increased. The increase in UHC and CO emissions was also observed for decreased nozzle holes.

[53] has conducted a numerical-experimental analysis that shows the effect of the injector nozzle tip Protrusion in a diesel engine running at high speed. The result shows a significant reduction in soot emissions, with no changes in other emissions and fuel consumption.

[54] has performed an experimental study to investigate the ignition delay and flame lift-off for different nozzle geometries having three different fuels and two different nozzle geometries. The study includes a conical nozzle and a cylindrical nozzle having an 8.6% larger outlet diameter than a conical nozzle. The author found that the cylindrical nozzle has reduced lift-off length with longer ignition delay as compared to the conical nozzle.

[55] has investigated the internal flows and spray formation for cylindrical and conical nozzle geometries in a diesel engine fuelled with three different fuels. The result showed slower spray tip penetration for the cylindrical nozzle. The surrogate fuel

mixture showed higher penetration than n-dodecane for the conical nozzle and lower penetration than n-dodecane for the cylindrical nozzle. The spreading angle was also greatly influenced by the nozzle geometry and the ambient density.

[56] has conducted a numerical study on the spray characteristics for different nozzle diameters (0.12mm and 0.2mm), injection pressure (40MPa, 70MPa, and 140MPa), and ambient temperature (500 K and 700 K). The result from the study shows that higher pressure had caused a smaller droplet diameter and a longer penetration length. Also, a smaller nozzle diameter leads to a shorter breakup length.

[57] has studied the effect of nozzle hole numbers (base-5 holes and modified-6 holes) on the fuel spray, wall impingement, and NO_x emissions. The authors have found that the NO_x emissions decrease for B20 fuel and 6-holes nozzle. However, the spray penetration length is smaller for B20 fuel and 6-holes nozzle and thus showed fewer chances of wall impingement.

[58] has performed a study to investigate the inner nozzle flow, spray, and combustion process for different nozzle geometries. The result showed a reduction in cavitation and turbulence within the nozzle orifice for conicity and hydro-ground nozzle. The soot emissions are maximum for the conical nozzle while the NO_x emissions are maximum for a hydro-ground nozzle.

[45] has performed an experimental analysis in a multi-cylinder diesel engine involving three injector nozzle geometries (six-hole, ten-hole, and six-hole convergent nozzle) having a high-pressure CRDI system. The authors found that NO_x and soot emissions reduce for all three injectors. The small nozzle having 10-hole has resulted in smaller fuel drops thus resulting in better atomization. It also showed better air utilization for

the smaller 10-hole nozzle that resulted in a decrease in the NO_x and soot emissions for wide operating conditions.

[59] investigated the combustion characteristics of a diesel engine for three nozzle hole layouts having baseline conventional nozzle and multi- and group-hole configuration. The result showed a reduction in CO and soot emissions using the group-hole nozzle for wide operating ranges. Also, the use of a multi-hole nozzle resulted in lower fuel consumption and CO emission for equivalent ratios (0.56 to 0.84) and injection timing of 15 °bTDC.

[60] has conducted a numerical and experimental study to investigate the performance and emission characteristics of a diesel engine for standard, convergent, and divergent nozzle hole geometry. The author has found lower NO_x emissions and higher soot for divergent nozzle geometry as compared to others. The numerical analysis also showed good compatibility for the prediction of emissions and agrees with the experimental data for all cases.

2.4 Spray Characteristics with varying nozzle geometry

[61] has conducted a study to analyze the spray mass and momentum development with different nozzle geometry (inlet rounding, converging-diverging, and straight-cylindrical) and operating conditions under high-pressure gasoline injection. The result showed an increase in mass flow rate for inlet rounding nozzle by 20% compared to straight cylindrical nozzles.

[62] has investigated the design factors for diesel spray with 20 different multi-hole nozzle geometries. The author has found the significant effect of orifice diameter on spray combustion. The vapor penetration has also been found to be an important design factor in the ignition delay period, ignition distance, and lift-off length.

[63] has studied the spray and combustion characteristics of a large two-stroke diesel engine for different nozzle geometry (6-orifice nozzle and 5-orifice nozzle; with and without hydro-erosive grinding). The result showed different behavior for the eccentric nozzle for its distinctive in-nozzle swirl cavitation pattern. This causes the improved start of ignition and wider spray angle.

[64] has performed an experimental and numerical study to investigate the orientation of injectors for efficient fuel spray patterns in a diesel engine. The orientation of the nozzle has been analyzed using CFD. The findings from the study showed injection and fuel spray characteristics have controlled the combustion and pollutant formation process. Also, 3 mm lift has shown a better velocity flow coefficient.

[40] conducted a numerical study on the spray formation in a diesel injector nozzle using Eulerian $\Sigma - Y$ coupled simulations for different nozzle eccentricity (0.50 to 0.94). The result showed improvement of discharge and area coefficients for horizontal elliptical nozzles with an increase in eccentricity because of lower cavitation. This also causes a vapor field to have lower intensity. However, for the spray characteristics, an increase of eccentricity in the nozzle caused improvement of air entrainment while reducing spray penetration. Furthermore, an increase in angle and jet entrainment was observed as the eccentricity increased which showed that the elliptical nozzle may improve the spray atomization processes.

[65] has investigated the characteristics of spray dynamics of a multi-hole diesel nozzle for the three, five, six, and nine-nozzle hole numbers. The investigation includes the employment of the X-Ray phase imaging technique. The author has found that increasing the hole numbers resulted in a non-linear trend in a spray structure. The

author has also suggested that for optimized engine combustion, great attention is required for predicting the number of holes in the nozzle.

[66] has analyzed the string cavitation and spray characteristics for different nozzle hole geometry using a high-speed CMOS camera. The results showed excitement in the instability of the spray cone angle due to string cavitation in the nozzle. This showed the larger contribution of string cavitation on the spray cone increment rather than nozzle geometry. The L/D ratio and sac types have also affected the string cavitation and spray characteristics.

[67] has conducted an experiment to analyze the internal flows and near nozzle spray behavior for different nozzle shapes. The experiment includes different mini-sac type nozzles, having different shapes of holes (cylindrical, convergent, and divergent) but similar hole diameters. The findings are the improved turbulence due to cavitation collapsed inside the hole, however, has lower effects on the spray cone angle. But the angle increased sharply if the cavitation extended to the hole outlet.

[58] has performed an experimental and computational study on the injector flows and spray simulations for different nozzle orifice geometries. The author has found reduced primary break-up and sprays dispersion while increased spray penetration for the nozzle with conicity and hydro-grinding because of the reduction in cavitation and turbulence inside the nozzle orifice. The vaporization process and air-fuel mixing are also found to be reduced. However, the flame-lift-off length and NO_x formations are found higher for the hydro-ground nozzle and lower for the conical nozzle.

2.5 Summary

The research work carried out in the past showed the advancement in the area of nozzle geometry. The research on nozzle geometries was started with the development of a 2-

D model to simulate it in a diesel engine. Many satisfactory results were observed in this area. The progress towards 3-D modeling has been achieved with the advancement in computer systems. Accurate predictions of the diesel engine's characteristics have been possible with the development of computer technologies. This development encourages taking up these complex 3-modeling on a personal computer. Furthermore, with the introduction of CRDI diesel engines, improvement in engine performance has been observed in many studies with varying nozzle geometry. However, as the emissions norms become more strict, it is required to achieve a better combustion process while reducing the emissions from a diesel engine. From the literature review, it is found that varying the nozzle geometries has shown great potential in improving the combustion process inside the diesel engine with the reduction in emission formations.

2.6 Research Gap

The in-depth literature review leads to the following research gap.

1. However, a detailed investigation has been carried out on the effect of nozzle hole diameter on the performance and combustion characteristics, its effect on the emission and spray characteristics is still a less-explored area.
2. Limited numerical studies have been employed for investigating the effect of nozzle hole diameter in the diesel engine.
3. The detailed investigation of the flow process inside the combustion chamber is still limited.

2.7 Objectives

The trailing research objectives have been delineated for the present research study.

1. Selection of suitable CFD software for the investigation.

Some studies on engine combustion, emission, and spray characteristics of a CRDI diesel engine with variable nozzle geometry using ANSYS

2. Selection of suitable sub-models in the software.
3. Numerically investigating the combustion, emission, and spray characteristics of the diesel engine fuelled with the diesel for different nozzle hole diameters.
4. Analyzing the optimized injection duration for different nozzle hole diameters.
5. Experimentally investigating the combustion characteristics of the diesel engine fuelled with the diesel for different nozzle hole diameters.
6. Numerical and experimental comparison of the combustion characteristics of the diesel engine for different nozzle hole diameters.
7. Combustion, emission, and spray characteristics of the diesel engine using the CFD software for different nozzle hole diameters.

CHAPTER 3

RESEARCH METHODOLOGY

3.1 Introduction

The basic principles and methodologies employed in this study are described in the present chapter. Initially, the ANSYS Forte is used to model the diesel engine. This simulation package is considered mainly to simulate the IC Engine designs. It provides a three-dimensional representation of the spray dynamics and combustion characteristics. The spray dynamics are governed by the turbulent mixing process and the chemical kinetics of fuel in a diesel engine. The utilization of ANSYS Forte effectively improves the accuracy of engine simulation within the commercial design limit. This is because of the presence of “chemistry solution techniques” in the ANSYS Forte that reduces the simulation time with respect to conventional CFD. The predictive simulation is possible through ANSYS Forte because of the controlled chemical kinetics with a multi-component fuel representation. Figure 3.1 shows the flow overview-High-level view of simulation tasks. ANSYS Forte marks a new standard by effective prediction of fuel-spray droplet breakup and vaporization in DI engines.

3.2 Basic Conservation Equations

3.2.1 Turbulent Reacting Flow

In the CI engine, the fluid flows are characterized to be turbulent, reactive, and multi-phase. The ANSYS Forte controls the representation of turbulent fluid flow through the fluid dynamics using the Navier-stokes equations. The mass-, momentum-, and energy conservation equations are used to represent the turbulent characteristics of the flow in

combination with the compressible as well as gas-phase flows. The exchange functions are utilized to simulate the fuel injection process in a diesel engine.

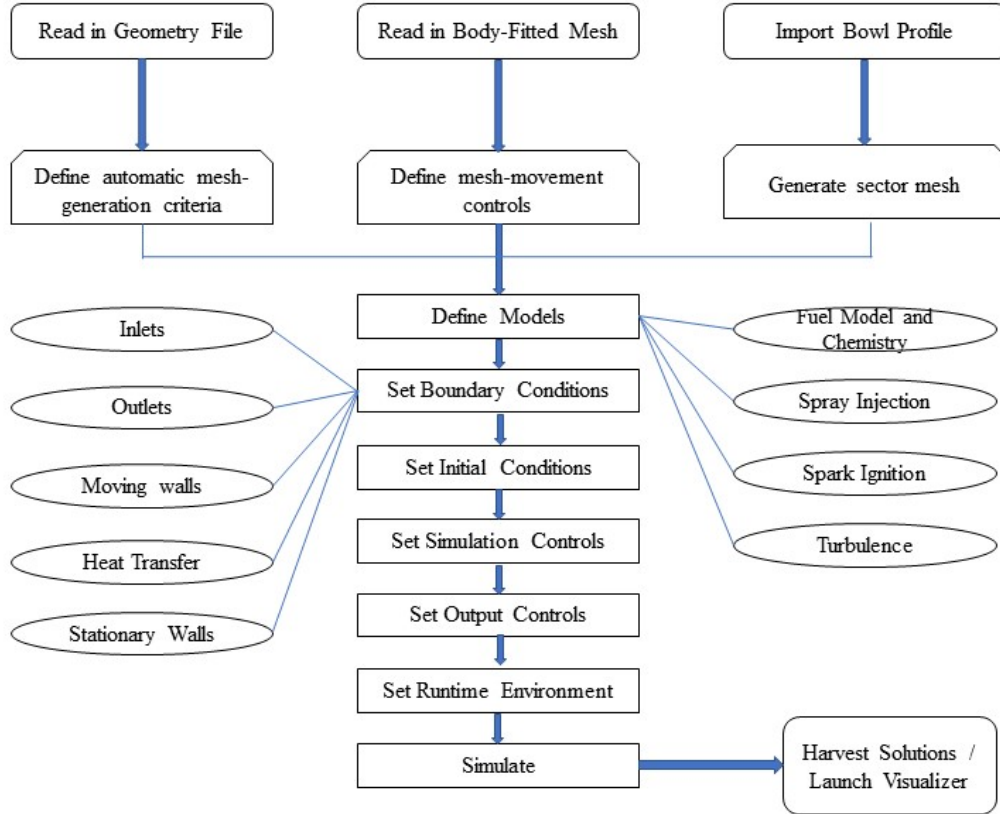


Figure 3.1. Flow Overview-High-level view of simulation tasks

3.2.1.1 Species-Conservation Equation

In the ANSYS Forte, the modeling of the working fluids is done as individual components/species. However, the flow convection, turbulent transport, molecular diffusion, and combustion cause the modification in components during the engine cycle. The mass conservation equation of species is:

$$\frac{\partial \bar{\rho}_k}{\partial t} = \nabla \cdot (\bar{\rho}_k \tilde{u}) = \nabla \cdot [\bar{\rho} D \nabla \bar{y}_k] + \nabla \cdot \phi + \dot{\bar{\rho}}_k^c + \dot{\bar{\rho}}_k^s \quad (3.1)$$

where ρ represents density, k represents species index ($k = 1, \dots, K$), K represents the species total number, D represents the molecular diffusion coefficient, u represents the flow-velocity vector, and $y_k = \frac{\rho_k}{\rho}$ represents the weight fraction. The term- ϕ undertakes the effects of total-averaged which has to be modeled.

3.2.1.2 Continuity Equation

The integration of the equation (3.1) for the entire k -species results in a continuity equation for total gas-phase fluid:

$$\frac{\partial \bar{\rho}}{\partial t} + \nabla \cdot (\bar{\rho} \tilde{u}) = \dot{p}^s \quad (3.2)$$

3.2.1.3 Momentum-Conservation Equation

The fluid-momentum equation is given by:

$$\frac{\partial \bar{\rho} \tilde{u}}{\partial t} + \nabla \cdot (\bar{\rho} \tilde{u} \tilde{u}) = -\nabla \cdot \bar{p} + \nabla \cdot \bar{\sigma} - \nabla \cdot \bar{\Gamma} + \bar{F}^s + \bar{\rho} \bar{g} \quad (3.3)$$

where p represents pressure, \bar{F}^s represents the change in the momentum rate, g represents specific force due to body weight, per unit mass, $\bar{\sigma}$ represents viscous shear stress.

3.2.1.4 Energy-Conservation Equation

The equation for internal energy transport is given by:

$$\frac{\partial \bar{\rho} \tilde{I}}{\partial t} + \nabla \cdot (\bar{\rho} \tilde{u} \tilde{I}) = -\bar{\rho} \nabla \cdot \bar{u} - \nabla \cdot \bar{J} - \nabla \cdot \bar{H} + \bar{\rho} \bar{\epsilon} + \dot{Q}^c + \dot{Q}^s - \dot{Q}_{rad} \quad (3.4)$$

where \tilde{I} represents internal energy, $\tilde{\varepsilon}$ represents turbulent kinetic energy dissipation rate, terms $-\dot{Q}^c$ and \dot{Q}^s represents the interaction of chemical heat release and spray, \dot{Q}_{rad} represents radiative heat loss and \bar{J} represent heat flux vector.

3.3 Turbulence Model

3.3.1 Reynolds-Averaged-Navier-Stokes (RANS) Model

This model is based on the average value of the flow field from the various realization of flows which resulted in the better transport and mixing of the fluid. The major advantage of using this model is the elimination to resolve small-scale structures in the flow realizations. However, the RANS methods retain the mean effect of turbulence on the flow field and combustion characteristics. For this model, the Reynolds stress tensor is given as:

$$\Gamma = -\bar{\rho}v_T \left[\nabla \tilde{u} + (\nabla \tilde{u})^T - \frac{2}{3} (\nabla \cdot \tilde{u}) I \right] + \frac{2}{3} \bar{\rho} \tilde{k} I \quad (3.5)$$

where v_T and \tilde{k} represents the turbulent kinetic-viscosity and -energy.

$$\tilde{k} = \frac{1}{2\bar{\rho}} \text{trace}(\Gamma) = \frac{1}{2} \tilde{u}'' \cdot \tilde{u}'' \quad (3.6)$$

The turbulent flux for species transport is expressed as:

$$\Phi = \bar{\rho} D_T \nabla \bar{y}_k \quad (3.7)$$

where D_T represents the turbulent diffusivity. Similarly, the term convective flux (H) is expressed as:

$$H = -\lambda_T \nabla \bar{T} - \bar{\rho} D_T \sum_k \tilde{h}_k \nabla \bar{y}_k \quad (3.8)$$

where λ_T represents the turbulent thermal conductivity.

$$D_T = \frac{\nu_T}{Sc_T} \quad (3.9)$$

$$\alpha_T = \frac{\nu_T}{Pr_T} \quad (3.10)$$

where Sc_T and Pr_T are Schmidt and Prandtl numbers for turbulent flows.

The basic as well as advanced $\kappa - \varepsilon$ models that are based on Re-normalized Group Theory are used in the ANSYS Forte. The standard Favre-averaged equations for κ and ε are expressed by:

$$\frac{\partial \bar{\rho} \tilde{k}}{\partial t} + \nabla \cdot (\bar{\rho} \tilde{u} \tilde{k}) \quad (3.11)$$

$$= -\frac{2}{3} \bar{\rho} \tilde{k} \nabla \cdot \tilde{u} + (\bar{\sigma} - \Gamma) : \nabla \tilde{u} + \nabla \cdot \left[\frac{(\mu + \mu_T)}{Pr_k} \nabla \tilde{k} \right] - \bar{\rho} \tilde{\varepsilon} + \overline{\dot{W}^s}$$

$$\frac{\partial \bar{\rho} \tilde{\varepsilon}}{\partial t} + \nabla \cdot (\bar{\rho} \tilde{u} \tilde{\varepsilon}) = -\left(\frac{2}{3} c_{\varepsilon 1} - c_{\varepsilon 3} \right) \bar{\rho} \tilde{\varepsilon} \nabla \cdot \tilde{u} + \nabla \cdot \left[\frac{(\nu + \nu_t)}{Pr_\varepsilon} \nabla \tilde{\varepsilon} \right] \quad (3.12)$$

$$+ \frac{\tilde{\varepsilon}}{\tilde{k}} (c_{\varepsilon 1} (\bar{\sigma} - \Gamma) : \nabla \tilde{u} - c_{\varepsilon 2} \bar{\rho} \tilde{\varepsilon} + c_s \overline{\dot{W}^s})$$

where $\overline{\dot{W}^s}$ represents the negative dispersing rate of turbulent eddies with the spray droplets. The values of $Pr_k, Pr_\varepsilon, c_{\varepsilon 1}, c_{\varepsilon 2}, c_{\varepsilon 3}$ are listed in Table 1.

Table 1. Values of the model constants.

	C_μ	$c_{\varepsilon 1}$	$c_{\varepsilon 2}$	$c_{\varepsilon 3}$	$1/Pr_k$	$1/Pr_\varepsilon$	η_0	β
Standard $\kappa - \varepsilon$	0.09	1.44	1.92	-1.0	1.0	0.769		
RNG $\kappa - \varepsilon$	0.08 450	1.42	1.68	$c_{\varepsilon 3}$ $= \frac{-1 + 2c_{\varepsilon 2} - 3m(n-1) + (-1)^\delta \sqrt{6} c_\mu c_\eta}{3}$	1.39	1.39	4.38	0.01 2

3.3.2 Large-Eddy Simulation (LES) Method

This method measures the individual flow realization. Unlike the RANS method, the LES method includes some unsteadiness and has smaller flow length scales. This method is employed to simulate only larger 3-D unsteady turbulent motions using the mesh resolution. In this method, the actual flow field resulted in the resolved flow field having a similar mesh size. LES methods do not require resolving flow scales lower than the filter size. The smaller filter mesh size resulted in the improved representation of turbulent flow-fields. The formulation between sub-grid scale (SGS) stress and flow field (filtered) strain rate is given by:

$$\Gamma = -\bar{\rho} v_{sgs} \left[\nabla \tilde{u} + (\nabla \tilde{u})^T - \frac{2}{3} (\nabla \tilde{u}) I \right] + \frac{2}{3} \bar{\rho} \tilde{k}_{sgs} I \quad (3.13)$$

The SGS viscosity, v_{sgs} , is formulated as:

$$v_{sgs} = (C_s \Delta)^2 S \quad (414)$$

where Δ represents the local mesh in CFD, S represents the amount of strain rate tensor filtered, and C_s represents a model constant.

The kinetic energy (\tilde{k}_{sgs}) for sub-grid is given by:

$$\tilde{k}_{sgs} = C_1 \Delta^2 S^2 \quad (3.15)$$

where C_1 represents a model constant. It can be seen that both v_{sgs} and \tilde{k}_{sgs} are dependent on the size of the mesh (Δ). The flux term (Φ) for the species transport is given as:

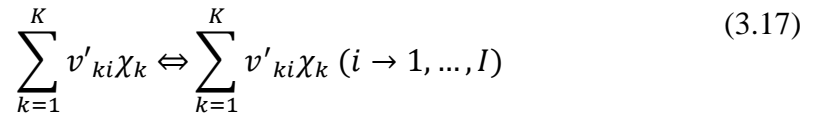
$$\Phi = \bar{\rho} D_{sgs} \nabla \bar{y}_k \quad (3.16)$$

where D_{sgs} represents the SGS turbulent diffusivity.

[68] has found that the dynamic structure has the advantage of better predicting the sub-grid stresses. Many researchers have validated the result of dynamic structure for the various flow problems [69], [70].

3.3.3 Formulation for Chemical Kinetics

The chemical kinetic mechanisms help in understanding the chemical reactions occurring during the combustion simulation. It characterizes the reaction rate and pathways that are associated with the change in the species concentration. [71] has formulated the detailed kinetic mechanism for reversible as well as irreversible reactions that involve k species, which is expressed as:



The relation between the production rate (ω_{ki}) and progress rate (q_i) for k^{th} species in the i^{th} reaction is given by:

$$\omega_{ki} = (v''_{ki} - v'_{ki}) q_i \quad (k \rightarrow 1, \dots, k) \quad (3.18)$$

The ANSYS Chemkin-pro present in Forte has the chemistry solver. The chemical source term ($\dot{\rho}_k^c$) is given as:

$$\dot{\rho}_k^c = W_k \sum_{i=1}^I \dot{\omega}_{ki} \quad (3.19)$$

where ω_{kr} represents the integration production rate for the entire reactions.

The heat release rate is given by:

$$\dot{Q}_c = - \sum_{i=1}^I Q_i q_i = \sum_{i=1}^I \sum_{k=1}^K (v_{ki}'' - v_{ki}') (\Delta h_f^0)_k q_i \quad (3.10)$$

where (Δh_f^0) represents the heat of formation for species “k” at zero degrees Kelvin.

3.3.4 Turbulent-Kinetics Interaction Model

The turbulent effects on combustion kinetics are modeled using the Turbulent-Kinetics Interaction Model. It is characterized by the mixing time-scale model that includes partly controlled combustion chemistry. The controlling of combustion chemistry is achieved using the disintegration of turbulent eddies that occurs because of improper fuel-oxidizer mixing during the combustion process. The effective rate of production for species “k” is given by:

$$\omega_{k,eff} = \frac{Y_{k,EQ} - Y_k}{\tau_{eff}} \quad (3.11)$$

where the relation between the effective time scale (τ_{eff}), chemical time sale (τ_{chem}) and turbulent scalar mixing (τ_{mix}) by:

$$\tau_{eff} = \tau_{chem} + \tau_{mix} \quad (3.12)$$

$$\tau_{mix} = C_{tki} \tau_{turb} = c_{tki} \frac{k}{\varepsilon} \quad (3.13)$$

The relation between $\omega_{k,eff}$ and $\dot{\omega}_k$ is given by:

$$\omega_{k,eff} \Delta t = Y_k^{n+1} - Y_k^n = \frac{\tau_{chem} \dot{\omega}_k \Delta t}{\tau_{eff}} = \frac{\tau_{chem} (Y_k^{kin} - Y_k^n)}{\tau_{chem} + \tau_{mix}} \quad (3.14)$$

The effective rate of species production used in kinetic integration is given by:

$$\omega_{k,eff} = \frac{\tau_{chem}}{\tau_{eff}} \dot{\omega}_k \quad (3.15)$$

3.4 Discretization Methods

3.4.1 Discretization - Governing Equations

This is done based on the control volume approach by considering the system as spatial coordinates. This approach allows accurate solutions with respect to time. In this, further discretization of the equations is performed using the “operator-splitting method”.

3.4.2 Temporal Differencing Method

Temporal differencing allows integrating the equations with respect to time. For this, a three-stage approach is utilized for a given time step.

1. **Stage 1-** In this stage, the chemistry, as well as spray source terms solutions are calculated based on the Lagrangian coordinates. This stage involves the movement of fluid and sprays droplets with the cells that undergo the process of collision and breakup.

2. **Stage 2-** In this stage, the terms related to the acoustic mode, mass, momentum, and energy-diffusion, and spray momentum are calculated in addition to the turbulence equations.
3. **Stage 3-** In this stage, the preserved flow field is relocated on the revised computational mesh as the wall started its motion. This stage is also named as rezone stage because the second stage mesh is shifted to the revised-mesh to obtain the solutions for convective transport.

3.4.3 Spatial Differencing Method

This method includes the hexahedrons meshing for the 3D geometries [72], [73]. The computational mesh includes the spatial regions composed of a cell, with the corners cells known as vertices. The motion of the piston and valve is achieved through the movement of the vertices in a defined manner., the differencing of momentum equations is done using the momentum cell. The primary velocities allocated at the vertices are given by:

$$u_{ijk} = u(x_{ijk}, y_{ijk}, z_{ijk}) \quad (3.16)$$

and, the thermodynamic quantities are primarily located at the cell centres as:

$$Q_{ijk} = Q(x_{ijk}^c, y_{ijk}^c, z_{ijk}^c) \quad (3.17)$$

where $Q = p, \rho, T, I, \text{ or } \rho_k$ as well as k and ϵ .

3.5 SIMPLE Method

In ANSYS Forte, the algebraic finite-volume equations are solved using the implicit methods that are obtained from the differencing methods. The benefits of using the implicit methods are,

1. During the calculation of unsteady or transient flows, the temporal accuracy instead of stability constraints limit the time-step size desired.
2. The large time steps can be used to quickly achieve steady states when temporal accuracy is not desired.

ANSYS Forte uses a modified SIMPLE method. It involves a two-step iterative approach to obtain the solutions of the flow-field variable. The need for velocities calculation at each time step is fulfilled through iterative time-advance pressure gradients that employ acceleration and velocities obtained from the pressure calculation. Similarly, this method solves the temperature from the calculated pressure.

3.5.1 Convective Flux Discretization

In the ANSYS Forte, convective terms are calculated using the explicit time-step sub-cycling that provides computational efficiency over the implicit methods.

3.5.2 Chemistry Solver

The ANSYS Forte can simulate the real mechanism of fuel combustion involving a large number of species and reactions with time effectiveness. This is possible due to the presence of a chemistry solver which includes unique solver components. The ANSYS Forte applies an advanced solution approach that substantially enhances the chemistry solution efficiency.

3.6 Spray and Break-up Models

In ANSYS Forte, different mathematical models are employed to calculate the spray mechanisms. The nozzle flow model determines the initial spray conditions while the KH-RT model determines the droplet break-up process. The models used to determine the nozzle sub-process provide the benefit of lesser dependency on the mesh size and time-step size.

3.6.1 Nozzle Flow Model

This model determines the instantaneous flow conditions across the nozzle that describes the initial conditions for the spray. The mean flow velocity of the liquid fuel entering the nozzle is given by:

$$U_{mean} = \frac{\dot{m}}{\rho_l A} = \frac{4\dot{m}}{\rho_l \pi D^2} \quad (3.18)$$

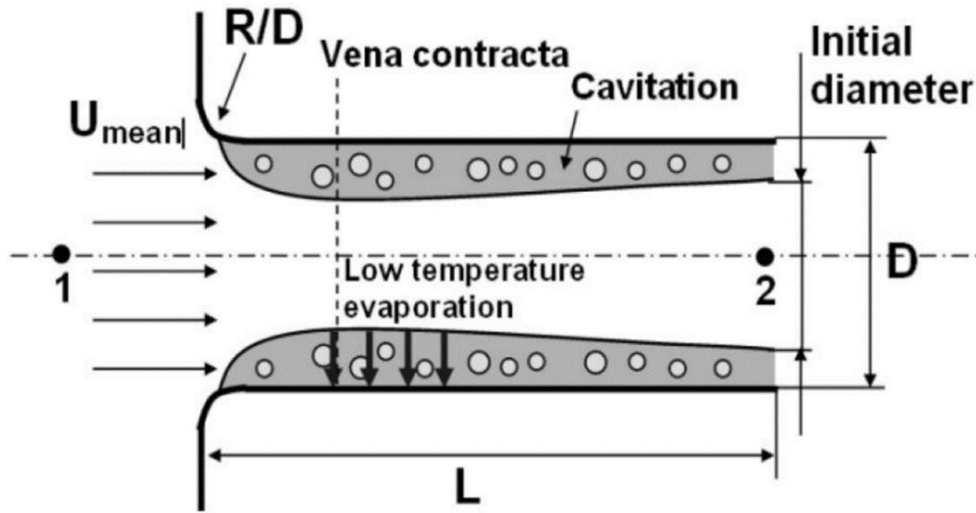


Figure 3.2. Flow-through nozzle passage [74]

The value of the mass flow rate given in equation (3.18) is smaller than the value of mass flow rate calculated using the Bernoulli Equation. This is due to the losses that occur because of acceleration of fuel, inlet velocity profile, wall friction, and expansion through the narrowest region (vena-contracta). To compensate for this loss, the discharge coefficient (C_d) is accounted which is given by:

$$C_d = \frac{U_{mean}}{\sqrt{2(p_1 - p_2)/\rho_1}} \quad (3.19)$$

where p_1 and p_2 are the pressure at locations 1 and 2 respectively as given in Figure

3.2. The inlet pressure p_1 , for turbulent flows is given by:

$$p_1 = p_2 + \frac{\rho_1}{2} \left(\frac{U_{mean}}{C_d} \right)^2 \quad (3.20)$$

The aerodynamic model determines the nozzle spray angle in combination with Taylor's analysis approach. It includes the analysis of the high-speed liquid break-up because of the variable growth of surface waves that result in the shedding of the liquid.

The spray angle (θ) is given as:

$$\tan \frac{\theta}{2} = \frac{4 \cdot \pi}{A} \cdot \sqrt{\frac{\rho_g}{\rho_l} \cdot f(T)} \quad (3.21)$$

where $A=C(L/D)$. The function $f(T)$ is given by:

$$f(T) = \frac{\sqrt{3}}{6} \cdot (1 - \exp(-10 \cdot T)) \quad (3.22)$$

$$T = \left(\frac{R_e}{W_e}\right)^2 \cdot \frac{\rho_l}{\rho_g} \quad (3.23)$$

3.6.2 Kelvin-Helmholtz / Rayleigh-Taylor (KH/RT) Break-up Model

It is a hybrid model which determines the process of spray atomization and droplet break-up [75], [76]. Figure 3.3 defines the working principle of the KH/RT break-up model in the ANSYS Forte. The KH model is applied for a specified length, known as the Break-up Length, measured from the tip of the nozzle (shown by region A). In this region, smaller droplets of the fuel get strips that are represented by parent parcels or "blobs". After the break-up length, both the KH and the RT models are applied to measure the secondary breakup process (shown by region B).

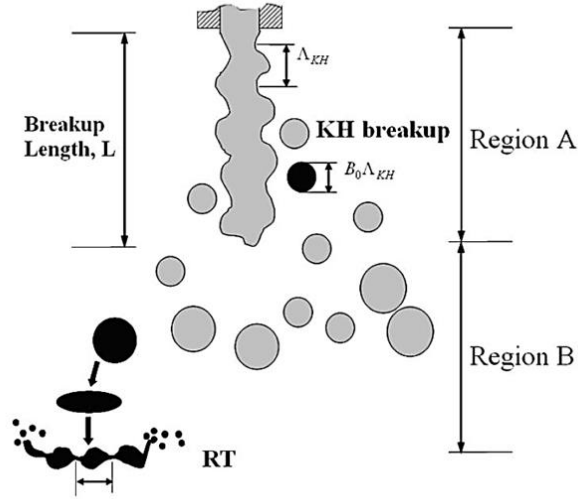


Figure 3.3. KH/RT break-up model for solid cone sprays [77].

3.6.3 KH Break-up Model

This model determines the primary breakup region of the fuel jet. It involves linear stability analysis which explains the disturbances that occur at a liquid-gas interface. For this, the model uses a Fourier series that allows the analysis of the break-up process. The rapid growth-rate of wave (Ω_{KH}) and its wavelength (Λ_{KH}) are given by:

$$\frac{\Lambda_{KH}}{r_p} = 9.02 \frac{(1 + 0.45Z^{0.5})(1 + 0.4T^{0.7})}{(1 + 0.87We_g^{1.67})^{0.6}} \quad (3.24)$$

$$\Omega_{KH} \left[\frac{\rho_l r_p^3}{\sigma} \right]^{0.5} = \frac{(0.34 + 0.38We_g^{1.5})}{(1 + Z)(1 + 1.4T^{0.6})} \quad (3.25)$$

where r_p represents the jet radius and σ represents the surface tension.

The Weber number (We_g) is given by:

$$We_g = \frac{\rho_g U_{rel}^2 r_p}{\sigma} \quad (3.26)$$

The radius of the new droplet formed during the primary break-up process is given by:

$$r_c = B_{KH} \Lambda_{KH} \quad (3.27)$$

where B_{KH} represents the size constant.

Some studies on engine combustion, emission, and spray characteristics of a CRDI diesel engine with variable nozzle geometry using ANSYS

The “blob injection” concept used in ANSYS Forte represents the injection of liquid-jet as an injection of parcels of blobs having a size similar to the effective nozzle diameter. The rate of change of parent droplet radius is expressed as:

$$\frac{dr_p}{dt} = -\frac{r_p - r_c}{\tau_{KH}} \quad (3.28)$$

The breakup time (τ_{KH}) is given by:

$$\tau_{KH} = \frac{3.726C_{KH}r_p}{\Lambda_{KH}\Omega_{KH}} \quad (3.29)$$

where C_{KH} represents the time constant.

The KH break-up model utilizes the two-step approach as shown in Figure 3.4. The first step involves the gradual reduction of parent droplet size (r_p) while the second step involves the formation of newer child parcels (r_c). The droplet numbers are assumed to be constant before and after the breakup. The droplet number (n_c) for child parcel and droplet size (r_p^{new}) for the parent parcel can be determined using two approaches:

I approach: It is based on the assumption that the parcel droplet size (r_p^{new}) is similar to the split child parcel (r'_p) size.

$$n_c = \frac{n_p(r_p^3 - r_p'^3)}{r_c^3} \quad (3.30)$$

II approach: This approach is based on the assumption that the SMD of the parent parcel is similar to the split child parcel. However, this approach resulted in a lower rate of brake-up with larger SMD.

$$n'_p r_p'^3 = n_c r_c^3 + n_p (r_p^{new})^3 \quad (3.31)$$

$$\frac{n_p (r_p^{new})^3 + n_c r_c^3}{n_p (r_p^{new})^2 + n_c r_c^2} \quad (3.32)$$

r'_p = The two equations can be combined into one for r_p^{new} as:

$$n_p (r_p^{new})^2 (r_p^{new} - r_c) = n'_p r_p'^2 (r'_p - r_c) \quad (3.33)$$

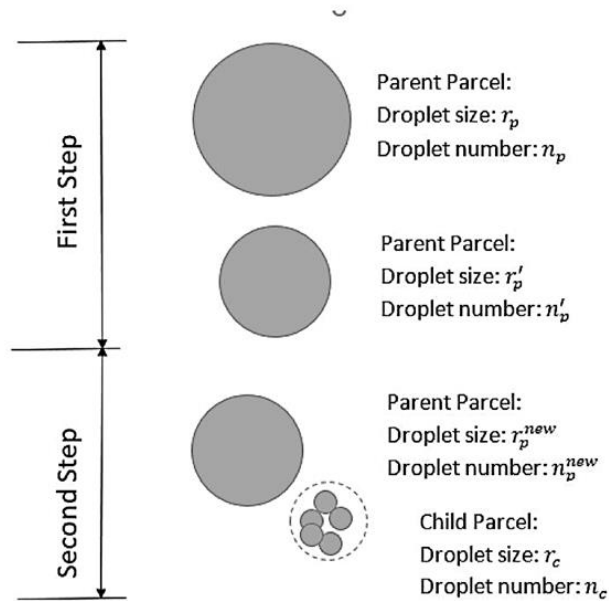


Figure 3.4. Two-step approach in the KH breakup model [74].

3.7 Simulation of Diesel Engine

The diesel combustion is simulated between the closing of the inlet valve to the opening of the exhaust valve. This is done because of the presence of exhaust gas-fuel mixture having a homogeneous nature just before the fuel injection. Also, the pattern for fuel injection nozzle holes is taken symmetry that depends on holes number. ANSYS Forte provides the advantage of utilizing the cylinder periodicity and hole pattern by representing a full geometry as a sector. In the current study, an eight-hole injector is simulated using a sector of 45° . The main advantage of using a sector of 45° is its smaller size that makes the simulation run faster than it would be with a 360° mesh.

3.7.1 Numerical Set-up

After defining the mesh, the models and solver options are set up using the ANSYS Forte. The simulation was carried out for a single-cylinder, four-stroke diesel engine running at a uniform speed of 1500 rev/min. The diesel fuel used in this simulation is

n-decane ($C_{10}H_{22}$) having properties similar to the diesel used during the experimental analysis. The different CFD sub-models used in the simulation of the engine are given in Table 2 with their physical significance.

Table 2: CFD sub-model

Physical phenomenon	Sub-model
Turbulence	RNG $\kappa - \varepsilon$ model [78]
Wall heat transfer	Model of Han and Reitz [79]
Spray breakup	Blob-Injection model [80]
Spray drag	Dynamic drag model [80]
Spray ignition	Shell model [81]
Combustion	Princeton combustion model [82]
NOx formation	Extended Zeldovich mechanism [83]

The specifications of the fuel injection system for the simulation of the engine are given in Table 3.

Table 3: Specification of Fuel Injection System

Nozzle hole diameter	Base- 0.20mm, Modified- 0.26mm & 0.30mm
Spray angle	125°
Start of Injection	22.5° bTDC
Discharge coefficient	0.7 (for all the three-injector nozzle)

3.7.2 Initial and Boundary Conditions

The simulation using the ANSYS Forte required the initial values for all the variables and fluid properties. The boundary conditions used in the simulation of the engine

include the injection pressure and fixed wall temperature. The values of initial and boundary conditions are given in Table 4.

Table 4. Initial and Boundary Conditions

Intake temperature	362 K
Injection fuel temperature	368 K
Intake pressure	2.215 bar
Piston temperature	500 K
Head temperature	470 K

3.7.3 Grid-Independence Test

[84] performed the numerical study in which the author has calculated the grid-independent solution using the in-cylinder pressure trends. The author has found that the grid refinement has no major effect on the result obtained so the results are considered independent of the grid. Thus, the current study is conducted using the second refinement level. Three different injector nozzle diameters are considered, i.e., 0.20mm, 0.26mm (base), and 0.30mm each having 8 numbers of the holes with 125⁰ included spray angles. Figure 3.5 shows the computational grid for the starting of the compression stroke.

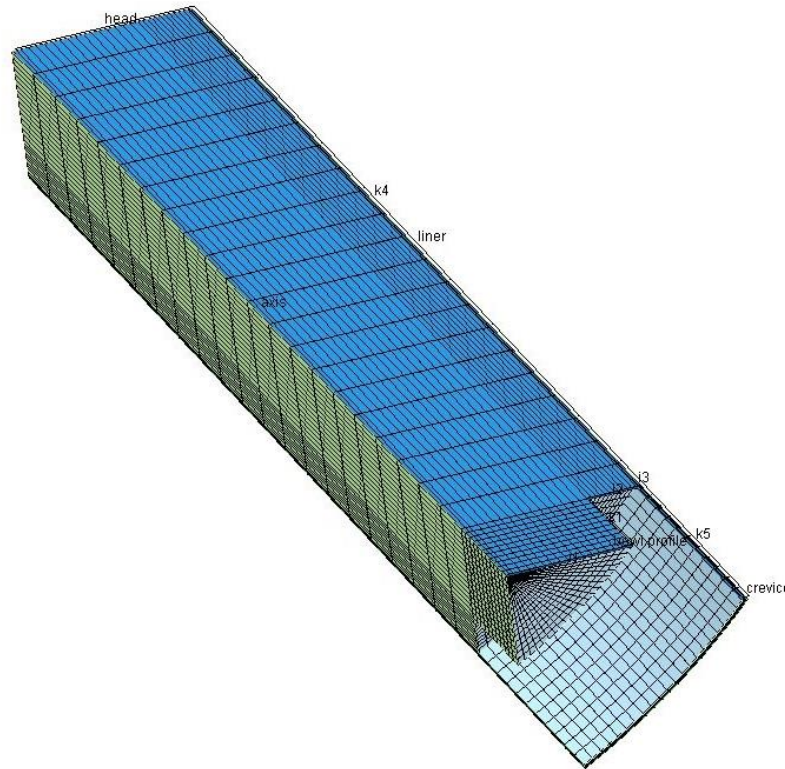


Figure 3.5. Computational Grid for Starting of Compression Stroke.

3.8 Selection of Test Engine

In the present study, the experimental analysis was performed on a single-cylinder, four strokes, CRDI-VCR diesel engine, running with a constant speed of 1500 rpm while developing 3.5 KW power and connected to an eddy current-based dynamometer. The engine specifications are provided in Table 5. The engine is capable of withstanding high pressure and is majorly employed in agriculture and industrial sectors. A test setup has the necessary instruments for the measurements of combustion pressure, temperature, load, fuel and air-flow, and crank-angle. The setup consists of the electronic control unit modeled Nira i7r that controls the solenoid injector. The injector can be driven using programmable ECU software and a calibration cable. The signals generated by the instruments are transferred to the computer using a high-speed data acquisition device. The cooling water is circulated in the water jacket using the pump

for engine cooling. Rotameters are used to measure the cooling water and calorimeter water flow within the engine.

Table 5. Test Engine Specifications

Type of engine and model	Single-cylinder, CRDI VCR, four-stroke, water-cooled
Stroke and Bore	110mm and 87.5mm
Idle speed	1500 rev/min
Injection Pressure	Up to 120 MPa (Variable)
Displacement Volume	661cm ³
Compression Ratio	12-18
Rated Power	3.5 KW
Type of Injector	Common rail Injector - Electronically Controlled
No. of Nozzle Holes	8
NHD	Base- 0.26mm, Modified- 0.20mm & 0.30mm
SOI	22.5 ⁰ bTDC

An open ECU-Nira i7r (see Figure 3.6) is equipped with the engine setup that controls the diesel engine with the efficient common rail technology. For monitoring the engine power, heat release, fuel consumption, and efficiencies of the diesel, a “Lab-VIEW” based EngineSoft software is used. With the application of this software, one can control the engine operating conditions. Advanced fuel injection systems and multiple injections can be achieved by using the Nira i7r. The EngineSoft in combination with the Nira i7r provides the system with having fast response time and effective control over the torque output.



Figure 3.6. ECU-Nira i7r Equipped with Engine Setup.

3.9 Selection of Engine Test Parameters

In this study, appropriate engine test parameters are selected judiciously. The testing of the engine was done in accordance with IS: 10000. The various test parameters that were selected for the analysis are given as:

1. Engine load
2. Engine speed
3. Fuel consumption rate
4. Temperature
5. In-cylinder pressure
6. NOx emissions
7. Heat release rate
8. Combustion duration

3.9.1 Measurement of Engine power

The brake power (BP) is considered the most crucial parameter in CI engine testing. In the present analysis, the engine employed is connected to an eddy current dynamometer (see Figure 3.7) through a flexible coupling. The dynamometer was employed for loading the engine and measuring the brake power at each load.



Figure 3.7. Eddy Current Dynamometer.

An eddy current dynamometer includes a stator and a rotor. The stator consists of permanent magnets whereas a disc of copper or steel is placed in a rotor. The rotor is connected to the engine shaft using the coupling. The electromagnets get energized by passing the current through them when the engine is loaded. As the rotor rotates, the eddy current is generated in the electromagnets that produce a magnetic field. This field opposes the rotor movement which loaded the engine. The amount of heat generated during the loading is carried away by the water passed through the dynamometer. The torque measurement is done through the moment arm and load cell type strain gauge that is employed in the dynamometer. By regulating the current in electromagnets, the

loading in the eddy current dynamometer is controlled. The engine brake power was displayed both on the control panel and the EngieSoft software. The calculation of brake power was done according to the following equation:

$$BP = \frac{2 * \pi * N(rpm) * Torque(N - m)}{60 * 1000} \quad (3.34)$$

3.9.2 Measurement of Engine Speed

The different rpm indicators are employed to measure the engine speed through a photosensor that generates the voltage pulses. The voltage pulses are sent for the conversion and the engine speed is displayed with an accuracy of ± 1 rpm. The engine speed was also displayed both on the control panel and the software.

3.9.3 Measurement of Fuel Consumption Rate

In the present study, only higher loads values are considered. However, the quantity of fuel consumed was measured at each load. The measurement of fuel consumption rate is done based on volume by utilizing a glass tube (burette) attached to the panel board and a stopwatch. The fuel consumption rate is calculated by considering the time taken for 10cc of the fuel consumed.

3.9.4 Measurement of Temperature

In the present study, Radix made, RTD type, PT100 (Type K) thermocouples made of chrome-alumel were utilized that is connected to a six-channel digital indicator to measure intake temperature, exhaust gas temperature, coolant water in and out temperature, and calorimeter water inlet and outlet temperature. The temperature indicator has been calibrated periodically by a millivolt source up to 800°C.

3.9.5 Measurement of In-cylinder Pressure

The in-cylinder pressure is measured using a piezoelectric transducer of “Kubeler” make. The signals obtained from the piezoelectric transducer were directed towards a

charge amplifier that amplifies the obtained signals and minimizes the signal noise. The signals are then directed to the data acquisition system which in combination with the signals obtained from the crank-angle encoder produces the pressure versus crank angle graph in the EngieSoft software. The pressure data were obtained for each crank angle degree rotation. In the present study, an average of fifty continuous cycles was considered for obtaining the in-cylinder pressure against the crank angle.

3.9.6 Calculation of Heat Release Rate

As the engine efficiency, power output, and emissions are greatly influenced by the heat release phenomenon, calculating the heat release rate during the combustion process is of great significance. Many researchers have performed the investigation using different models for determining the heat release rate. However, in the present study, the model utilizing the 1st law of thermodynamics is employed that is described in [25]. The model is a single-zone model which means there is no distinction between the burned and unburned zones present inside the cylinder at the time of combustion. Although multiple-zone models exist, the single-zone model is used instead of the multi-zone model as it provides the track of the unburned and burned areas for calculating the heat transfer. It was found in the previous studies that employing the multi-zone model does not offer larger benefits because of the uncertainties in defining the zones evolution [85]. The heat release rate is given by:

$$\frac{dQ}{d\theta} = \frac{1}{\gamma - 1} v \frac{dP}{d\theta} + \frac{\gamma}{\gamma - 1} P \frac{dv}{d\theta} - \frac{dQ_w}{d\theta} \quad (3.35)$$

where $\frac{dQ}{d\theta}$ represents the AHRR ($J/^\circ CA$), P represents the in-cylinder pressure (bar), γ represents the ratio of specific heat, and v represents the volume of a cylinder (m^3), θ represents the crank angle ($^\circ$), $\frac{dQ_w}{d\theta}$ represents the rate of heat transfer from the wall ($J/^\circ CA$).

3.10 Modification of Fuel Injection System (FIS)

The fuel injection system used in the engine is an electronically-controlled solenoid-operated common rail injector with a pressure sensor and pressure regulating valves. [3], [86] has found that the FIS significantly influences the flow process inside the combustion chamber. The main work of the FIS is to deliver the fuel in an appropriate quantity to the engine. The demand for the fuel in an engine depends upon its speed and load at every cycle. Therefore, another role of the FIS is to make sure that the engine will run smoothly and economically. The fuel is injected into the combustion chamber through single- or multi-holes present at the tip of the nozzle injector. The large pressure difference across the nozzle orifice delivers the fuel into the combustion chamber. [87] has found that the higher injection pressure resulted in improved spray characteristics in a diesel engine. The higher injection pressure assists in the proper atomization of the fuel injected into the combustion chamber because of its high velocity. The schematic representation of the FIS is shown in Figure 3.8. The fuel is delivered to the injector nozzle from the fuel tank at high pressure with the help of the supply pump. The leftover fuel is sent back to the fuel tank. The important component of the FIS is the injector nozzle. The injector nozzle employed in the present study has a diameter of 0.20mm, 0.26mm, and 0.30mm, each having 8 holes and 125° included spray angle. The base injector nozzle has a 0.26mm hole diameter while the modified injector nozzles have 0.20mm and 0.30mm hole diameter. The base nozzle used in the study is shown in Figure 3.9. The engine operates with a uniform speed of 1500 rev/min with constant fuel consumption of pure diesel and has a compression ratio of 17.5:1.

determined using the valve closure duration. The accurate prediction regarding the characteristics of the injected fuel in the injection system requires complex hydraulic models [25]. However, in the present study, an approximate estimation of the injection rate within the injector nozzle was considered. In this, the fuel flow is considered to be incompressible, one-dimensional, and quasi-static in nature. The fuel mass flow rate injected through the nozzle (\dot{m}_f) is given by:

$$\dot{m}_f = C_D A_n \sqrt{2\rho_f \Delta p} \quad (3.36)$$

where A_n represents the minimum nozzle area, C_D represents the discharge coefficient, ρ_f represents the fuel density, and Δp represent the drop of pressure across the nozzle. However, when the pressure drop is constant for the fuel injection period, then the fuel mass flow rate injected through the nozzle is given by:

$$\dot{m}_f = C_D A_n \sqrt{2\rho_f \Delta p} \frac{\Delta\theta}{360N} \quad (3.37)$$

where $\Delta\theta$ represents the period for which the nozzle opens (in crank angle degrees) and N represents engine speed (in rpm).

3.11 Experimental Trial Procedure

Initially, with no load-condition, the engine was operated for some time fuelled with the neat diesel. After the engine achieved the steady-state condition, readings at each load were taken. The calibration of every instrument was done periodically. The injection pressure was set at 90 MPa throughout the experiments. The engine load was increased gradually to full load. However, for the present study, only the readings at full loads are considered. At the full load conditions, the fuel/air mass flow rate, coolant temperature, and NOx emission were recorded for the engine. For recording the in-cylinder pressure versus crank-angle data, an average of fifty continuous cycles was

considered. The data were recorded using the data acquisition system and EngieSoft software.

3.11.1 Test for finding the Optimized injection duration

From the previous literature studies [88]–[90], it is found that varying the nozzle geometry varies the amount of fuel injected into the combustion chamber. Therefore, to compensate for this, an optimized injection duration was evaluated using the CFD analysis. This ensures the development of the same power for different injector nozzles in the engine. The evaluation of the optimized injection duration was done based on maximum brake power obtained during the CFD analysis employing different nozzle hole diameters. To obtain the brake power, the simulation of the diesel engine was performed for varying injection durations (20°, 25°, and 30° crank angles) while the SOI was 22.5° bTDC. Table 6 shows the parameters tested using the numerical as well as experimental analysis.

Table 6. Parameters For Finding Optimized Injection Duration

Nozzle Hole Diameter (mm)	SOI (°CA)	Injection Duration (°CA)	Engine Speed (rpm)
0.20	22.5	20	1500
		25	1500
		30	1500
0.26	22.5	20	1500
		25	1500
		30	1500
0.30	22.5	20	1500
		25	1500
		30	1500

3.12 Instruments Accuracy and Uncertainty in Measurement

The accuracy, as well as the uncertainty for the physical instruments used in this study, are shown in Table 7. All the instruments have higher accuracy.

Table 7. Physical Instrument Accuracy

Measurement	Principle of Measurement	Instrument Range	Accuracy
Pressure	Piezoelectric	0-2000 bar	$\pm 1 \text{ bar}$
Exhaust gas temperature	RTD/K-type thermocouple	0-1000 °C	$\pm 1 \text{ }^\circ\text{C}$
Crank angle sensor	Optical	0-720 °CA	$\pm 0.2 \text{ }^\circ\text{CA}$
Engine Load	Load cell type strain gauge	0-50 kg	$\pm 0.1 \text{ kg}$
Fuel Flow Transmitter	DP transmitter	0-500 mm	$\pm 1\%$

Whenever any quantity is measured, the results are always slightly different from their true values even when the experiments are performed carefully. This measurement error may either be systematic or random. The systematic error can be eliminated by adding the correction factor. However, the random errors cannot be easily predicted in advance and thus can only be statistically estimated. The random errors are observed in the result because of the multiple measurements for similar quantities under similar conditions. The uncertainty of the instrument is evaluated using the Gaussian distribution method. It has a confidence level of $\pm 2\sigma$. In the present study, the uncertainty is evaluated using the equation:

$$\Delta X = \frac{2\sigma_i}{\bar{X}} * 100 \quad (3.38)$$

Experiments were conducted to evaluate the mean (\bar{X}) and the standard deviation (σ_i) of any measured parameter. From the measured parameter, the uncertainty is computed by the method given by [91].

Let R be the computed quantity from 'n' independent measured parameters.

$$X_1, X_2, X_3, X_4 \dots \dots X_n$$

$$R = R(X_1, X_2, X_3, X_4 \dots \dots X_n) \quad (3.39)$$

Uncertainty limits for the measured parameter are given by:

$$X_1 + \Delta X_1, X_2 + \Delta X_2, X_3 + \Delta X_3, X_4 + \Delta X_4, \dots X_n + \Delta X_n$$

The uncertainty limit for the computed parameter is given by $R + \Delta R$

The principle of the root-sum-squared method is employed for calculating the realistic error limits for any computed quantity based on several measured quantities. The uncertainty of given operating conditions can be calculated by:

$$\Delta R = SQRT \left(\left(\frac{\partial R}{\partial X_1} * \Delta X_1 \right)^2 + \left(\frac{\partial R}{\partial X_2} * \Delta X_2 \right)^2 + \dots \left(\frac{\partial R}{\partial X_n} * \Delta X_n \right)^2 \right) \quad (3.40)$$

The overall uncertainty of the experiments was measured to be $\pm 3.7\%$.

CHAPTER 4

RESULT AND DISCUSSION

4.1 Introduction

ANSYS Forte CFD package utilizes the ANSYS Chemkin-Pro solver technology for the simulation that reduces the efforts spent on manual mesh preparation. Forte consists of Automatic-Mesh-Generation (AMG), Adaptive-Mesh-Refinement (SAM) solution, and geometry-based Adaptive-Mesh-Refinement (AMR). Forte utilizes the multi-component models in combination with comprehensive spray dynamics without any effect on the simulation time [74]. The accurate simulation of combustion performance for any fuel is the major advantage of Forte. This ensures the engineers design the cleaner engine with higher efficiency, and fuel flexibility with lesser simulation time. The automatic mesh generator in Forte provides the benefits of analyzing the simulation design without generating any mesh.

In the past, the use of the CFD model has proven to be a potential way for analyzing the in-depth characteristics of IC engines [92]–[94]. This chapter details the results of the numerical analysis for the combustion, emission, and spray characteristics with different nozzle hole diameters. The numerical investigation was carried on an ANSYS Forte CFD simulation package for the same engine and injection details as that of the experimental engine.

4.2 OPTIMIZED INJECTION DURATION

The two parameters used for the evolution of optimized injection duration are brake power and NO_x emissions. The selection of optimized injection is done for the maximum brake power obtained for the engine. The optimized injection durations

obtained from the CFD analysis are 30° CA for 0.20 mm, 25° CA for 0.26 mm, and 20° CA for 0.30 mm. Later, the values of optimized injection duration from the CFD analysis are validated by operating the test engine with these values. The variation in the injection duration on the test engine was done using EngineSoft through the ECU-Nira i7r attached to the test-engine setup. The results obtained from the experimental analysis are found within the range of the CFD results. This validated the optimized injection duration obtained from the CFD analysis. Also, the NOx emissions are found to be within the acceptable range for the evaluated optimized injection duration. The comparison for experimental and CFD analysis for different nozzle hole diameters at optimized injection duration is shown in Table 8.

Table 8: Comparison for experimental-CFD analysis at optimized injection duration for different nozzle hole diameter

(a) For brake power					
Nozzle hole diameter (in mm)	Injection timing (°bTDC)	Injection duration (°CA)	Brake power (in KW) (CFD analysis)	Brake power (in KW) (Experimental analysis)	Error (in %)
0.20	22.5	30	3.34	3.36	0.59
0.26	22.5	25	3.30	3.34	1.19
0.30	22.5	20	3.29	3.30	0.30
(b) For NOx emissions					
Nozzle hole diameter (in mm)	Injection timing (°bTDC)	Injection duration (°CA)	NOx (in ppm) (CFD analysis)	NOx (in ppm) (Experimental analysis)	Error (in %)
0.20	22.5	30	318	320	0.63
0.26	22.5	25	197	200	1.52

0.30	22.5	20	98	100	2.04
------	------	----	----	-----	------

4.3 VALIDATION OF NUMERICAL ANALYSIS

Firstly, the validation of the results obtained from the CFD analysis is done on the basis of the result obtained from the experimental analysis. The validation of numerical analysis is done to predict the accuracy of the sub-model utilized in the study.

4.3.1 COMPARISON OF NUMERICAL ANALYSIS AND EXPERIMENTAL ANALYSIS

Figure 4.1 compares the CFD analysis and experimental analysis results of in-cylinder pressure obtained for (a) 0.20 mm, (b) 0.26 mm, and (c) 0.30 mm nozzle hole diameter respectively. Good compatibility was observed between the CFD analysis and experimental analysis for all the nozzle hole diameters used in the study. The experimental result of the peak in-cylinder pressure for 0.26 mm nozzle hole diameter is found to be 8.12 MPa. Whereas, the numerical analysis result of the peak in-cylinder pressure for 0.26 mm nozzle hole diameter is found to be 7.91 MPa. The minor differences are observed near 7.75° bTDC that is after the injection has started and at the peak pressure. Other than this, the CFD models showed good predictability over the entire crank angle interval. The reason for good compatibility may be the application of multi-zone models employed in the current study that offers a good representation of the spatial distribution of fuel-flow characteristics and temperature inside the combustion chamber.

Figure 4.1 also compares the CFD analysis and experimental analysis of the apparent heat release rate for (a) 0.20 mm, (b) 0.26 mm, and (c) 0.30 mm nozzle hole diameter respectively. Similar to the in-cylinder pressure, the comparison for AHRR has also

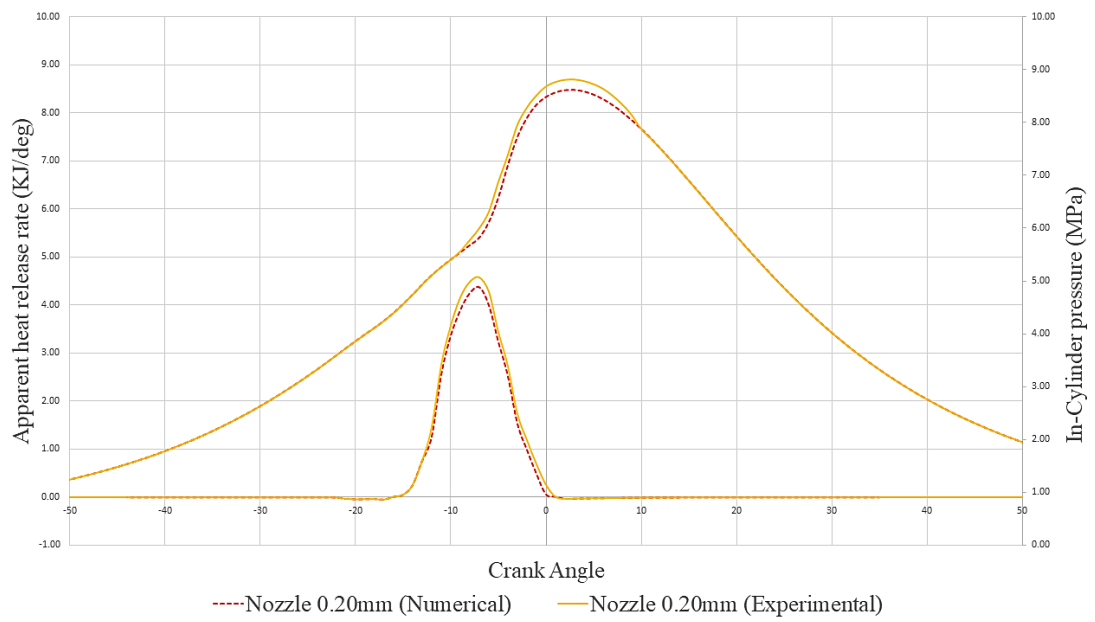
shown good compatibility. The experimental result of the AHRR for 0.26 mm nozzle hole diameter is found to be 3.88 KJ/deg while the numerical analysis result of the AHRR for 0.26 mm nozzle hole diameter is found to be 3.58 KJ/deg. The presence of a chemistry solver in the ANSYS Forte predicted the absorption and release of heat during the reaction when the chemical species such as NO_x and CO are dissociated and re-associated in the chemical reactions. The amount of heat that had been absorbed during the dissociation of the chemical species has been restored at the time of re-association of the chemical species [11].

The comparison for other nozzle hole diameters has also shown the variation similar to the 0.26 mm nozzle hole diameter. The relative error for numerical-experimental in-cylinder pressure and AHRR obtained for different nozzle diameters at a particular crank angle degree is calculated to verify the authenticity of the results. The calculated relative error is shown in Table 9.

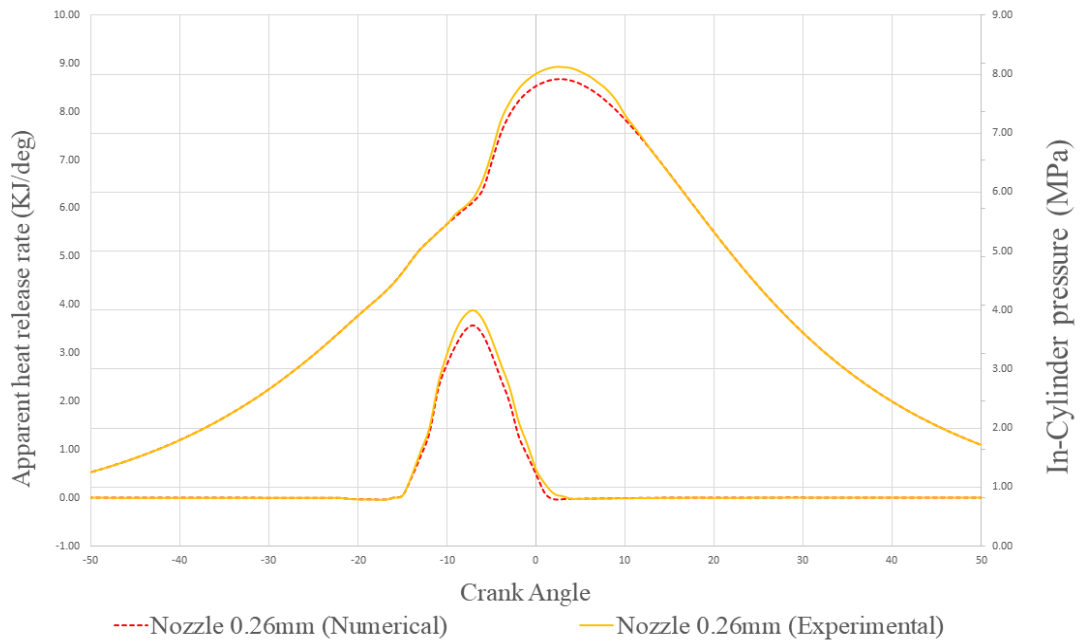
Table 9. Relative error for numerical-experimental (a) In-cylinder pressure and (b) AHRR at a particular crank angle degrees.

(a) In-Cylinder Pressure				
NHD (in mm)	Crank Angle Degree (°CA)	Experimental In-Cylinder Pressure (in MPa)	Numerical In-Cylinder Pressure (in MPa)	% Error
0.20	5 ⁰ bTDC	6.87	6.57	4.34%
	3 ⁰ ATDC	8.81	8.61	2.27%
0.26	5 ⁰ bTDC	6.67	6.51	2.39%
	3 ⁰ ATDC	7.91	8.12	2.58%
0.30	5 ⁰ bTDC	6.60	6.40	3.03%
	3 ⁰ ATDC	7.79	7.59	2.56%

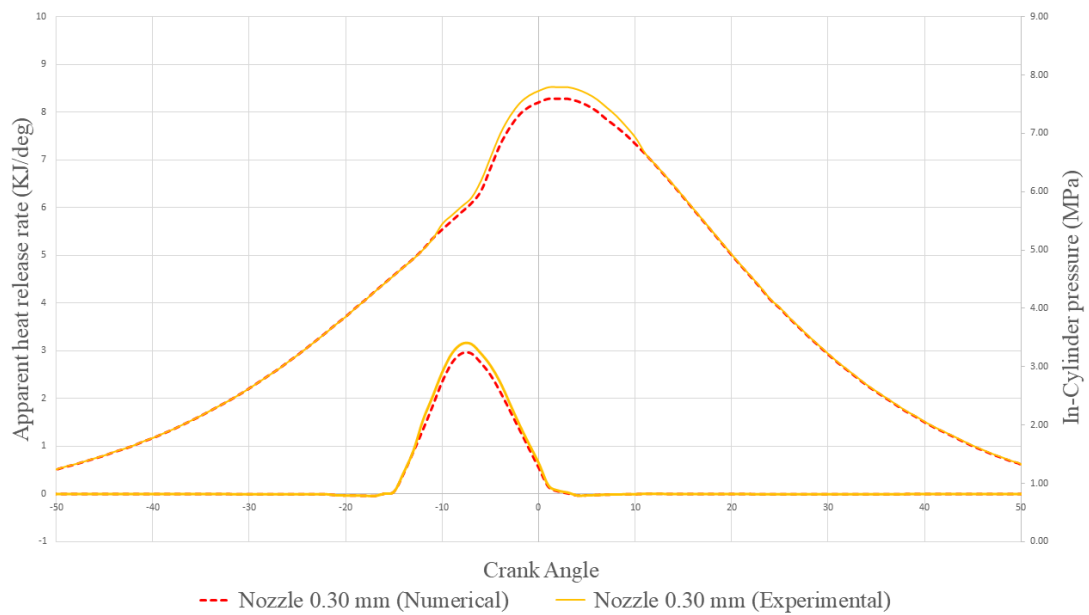
(a) AHRR				
NHD (in mm)	Crank Angle Degree (°CA)	Experimental AHRR (in MPa)	Numerical AHRR (in MPa)	% Error
0.20	12 ⁰ bTDC	1353	1257	7.09%
	5 ⁰ bTDC	3451	3247	5.91%
0.26	12 ⁰ bTDC	1447	1353	6.49 %
	5 ⁰ bTDC	3271	2991	8.56 %
0.30	12 ⁰ bTDC	1556	1444	7.19%
	5 ⁰ bTDC	2735	2593	5.19%



(a)



(b)



(c)

Figure 4.1. CFD analysis and experimental analysis comparison for the in-cylinder pressure and AHRR for (a) 0.20 mm nozzle hole diameter (b) 0.26 mm nozzle hole diameter, and (c) 0.30 mm nozzle hole diameter.

4.4 EFFECT OF NOZZLE HOLE DIAMETERS – NUMERICAL ANALYSIS

The application of the CFD model has shown great potential for detailed analysis of the diesel engine characteristics having different operating parameters without any requirement for the experimental data.

4.4.1 NUMERICAL INVESTIGATION OF THE ENGINE COMBUSTION CHARACTERISTICS

4.4.1.1 In-cylinder Pressure

The in-cylinder pressures for three nozzle hole diameters are portrayed in Figure 4.2. The peak in-cylinder pressure for 0.20 mm, 0.26 mm, and 0.30 mm nozzle hole diameter is found to be 8.61MPa, 7.91MPa, and 7.59MPa, respectively. Due to the formation of smaller size fuel droplets from the 0.20 mm nozzle hole diameter, the maximum peak for in-cylinder pressure is observed for this nozzle hole diameter. The smaller fuel droplets enhance the process of fuel atomization and vaporization which consequently results in better air-fuel mixing inside the combustion chamber. The improved mixing causes the air-fuel charge to combust properly which results in the elevated gas temperature. However, as the nozzle hole diameter increases, the peak in-cylinder pressure decreases due to the formation of a relatively larger size of fuel droplets. Another interesting point to observe is the delayed ignition period for smaller nozzle hole diameter because of proper air-fuel mixing. The peak in-cylinder is observed to be reduced by 8.31% and 11.85% respectively, for 0.26 mm and 0.30 mm nozzle hole diameter as compared to 0.20 mm nozzle hole diameter.

4.4.1.2 Apparent Heat Release Rate

The variation of AHRR for three nozzle hole diameters is portrayed in Figure 4.2. The peak AHRR for 0.20 mm, 0.26 mm, and 0.30 mm nozzle hole diameters are found to

be 4.37 KJ/deg, 3.58 KJ/deg, and 2.95 KJ/deg, respectively. The formation of smaller fuel droplets from the 0.20 mm nozzle hole diameter causes proper air-fuel mixing and thus leads to rapid combustion of charge present inside the combustion chamber. This causes a maximum peak heat release rate for 0.20 mm nozzle hole diameter. However, as the diameter increases, the flatter and broader shape of the AHRR is observed. During the initial phase, a negative trend in the AHRR is observed because of the endothermic reaction of the fuel with high-pressure high-temperature air. As seen from the figure, the AHRR is observed to be reduced by 11.82% and 32.55%, respectively for 0.26 mm and 0.30 mm diameter compared to 0.20 mm nozzle hole diameter. The results obtained are similar to the findings in the previous literature [95], [96] where the smaller orifice resulted in rapid atomization of fuel, faster evaporation, and thus better fuel-air mixing.

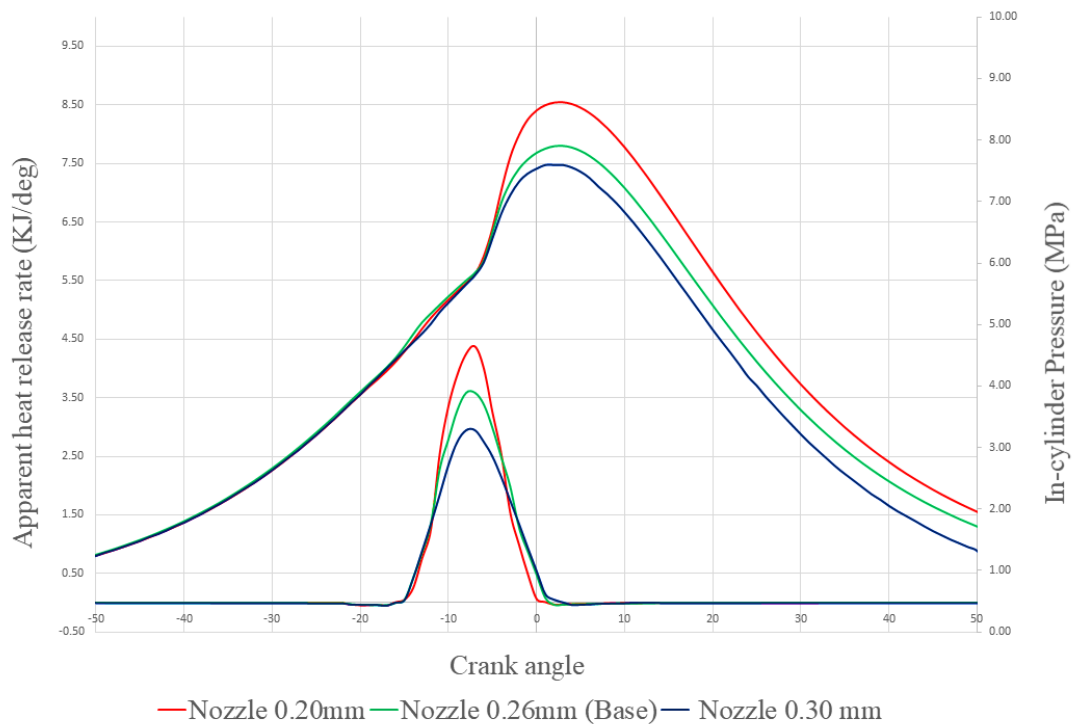


Figure 4.2. Peak In-cylinder pressure and AHRR for 0.20 mm, 0.26 mm, and 0.30 mm nozzle hole diameter – Numerical Investigation

4.4.2 NUMERICAL INVESTIGATION OF THE ENGINE EMISSION CHARACTERISTICS

4.4.2.1 Unburnt Hydrocarbon Emissions

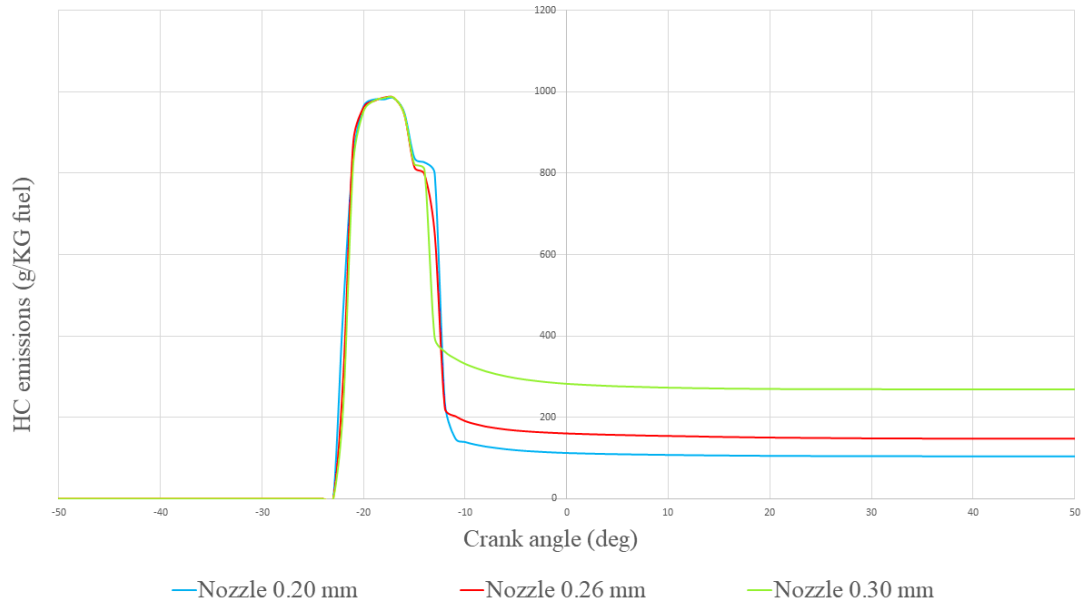


Figure 4.3. Variation of unburnt hydrocarbon emission for three different nozzle hole diameters.

Figure 4.3 portrays the variation of unburned hydrocarbons emissions for three nozzle hole diameters. It can be seen that as the nozzle hole diameter increases, the hydrocarbon emission also increases. [97] has found that the hydrocarbon emissions increase with the increase in the fuel droplet size. An increase in the size of fuel droplets causes improper air-fuel mixing as well as improper evaporation that makes the injected fuel escaped from the combustion zone. This escaping from the combustion zone leads to incomplete combustion. From the figure, it was found that hydrocarbon emissions increased by 29.90% and 60.13%, respectively for 0.26 mm and 0.30 mm diameter compared to the 0.20 mm nozzle hole diameter. Also, the AHRR is higher for 0.20mm

nozzle hole diameter, which may also have led to lower hydrocarbon emissions. [96] has also found a similar trend for hydrocarbons with increasing nozzle hole diameters.

4.4.2.2 Carbon Monoxide Emissions

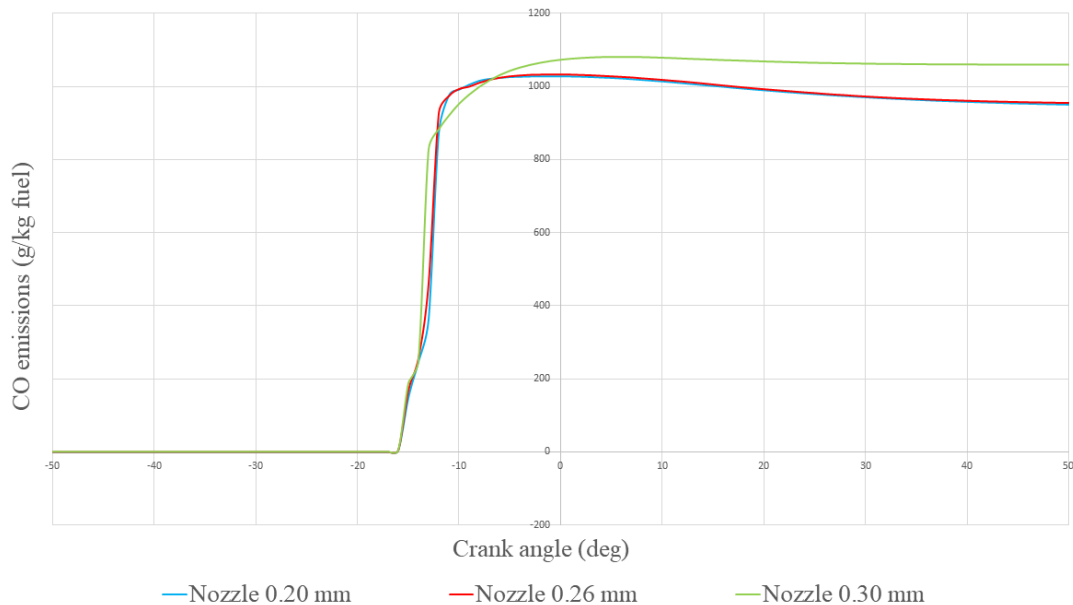


Figure 4.4. Variation of carbon monoxide emission for three different nozzle hole diameters.

Figure 4.4 portrays the variation of CO emissions for three nozzle hole diameters. It can be seen that as the nozzle hole diameter increase, the CO emissions also increase. The CO emissions are formed due to the partial combustion of hydrocarbons compounds. The increase in the size of fuel particles results in the improper atomization of the fuel inside the combustion chamber. This forms the local fuel-rich zones inside the combustion chamber because of improper air-fuel mixing. This overall causes partial (incomplete) combustion. From the figure, it was found that CO emissions increased by 0.65% and 5.08% respectively for 0.26 mm and 0.30 mm diameter compared to the 0.20 mm nozzle hole diameter. The results obtained for hydrocarbons and CO emissions are similar to the findings in previous literature [95], [96].

4.4.2.3 Nitrogen Oxide Emissions

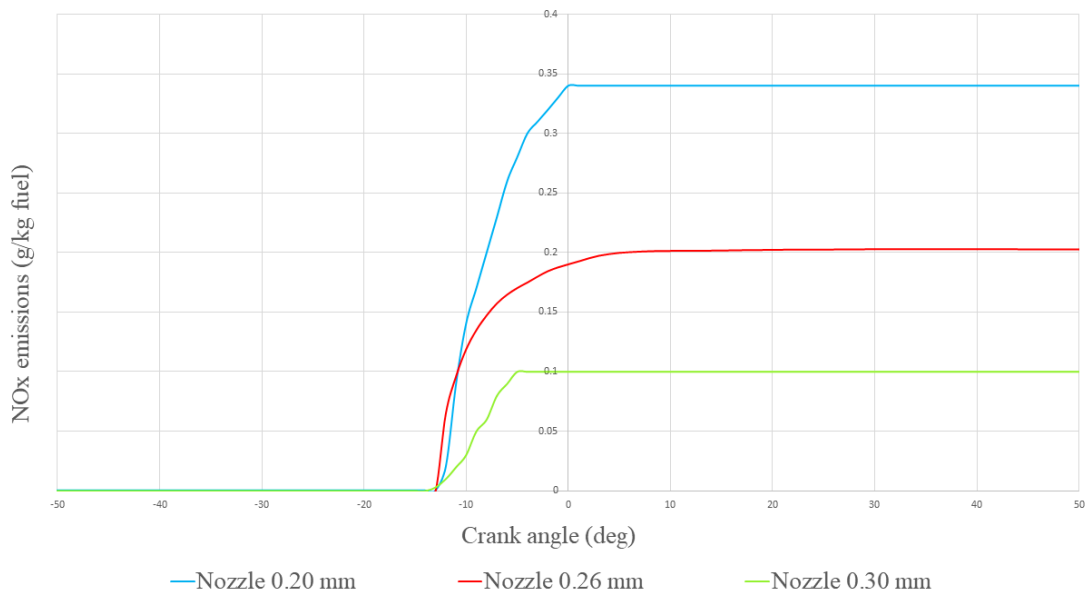


Figure 4.5. Variation of nitrogen oxide emission for three different nozzle hole diameters.

Figure 4.5 portrays the variation of nitrogen oxides for three nozzle hole diameters. The decrease in the NO_x emissions is observed for increasing nozzle hole diameters. The NO_x formation can be influenced by the combustion temperature, availability of time for chemical reactions, and availability of oxygen-rich zones [98]. The reaction of the N molecule with the hydrocarbons radicals resulted in the formation of NO_x emissions within the fuel-rich flame zone. Fuels containing nitrogen are also responsible for NO_x formation. The extended Zeldovich mechanism is used to describe the process of NO_x formation [99], [100]. From the figure, the decrease in NO_x emissions was observed by about 41.18% and 70.58% respectively for 0.26 mm and 0.30 mm diameter compared to 0.20 mm nozzle hole diameter. Reduction in the premixed combustion period with increasing hole diameter causes the reduction in combustion temperature that reduces the NO_x emissions formation. The larger fuel droplet size causes the reduction of the

ignition delay period thus minimizing the fuel-air mixing duration causing a lower rate of heat release during the initiation of the combustion process. [96], [97] has also found similar trends for NO_x emissions with different nozzle diameters.

4.4.3 NUMERICAL INVESTIGATION OF THE ENGINE SPRAY CHARACTERISTICS

4.4.3.1 Liquid Penetration Length

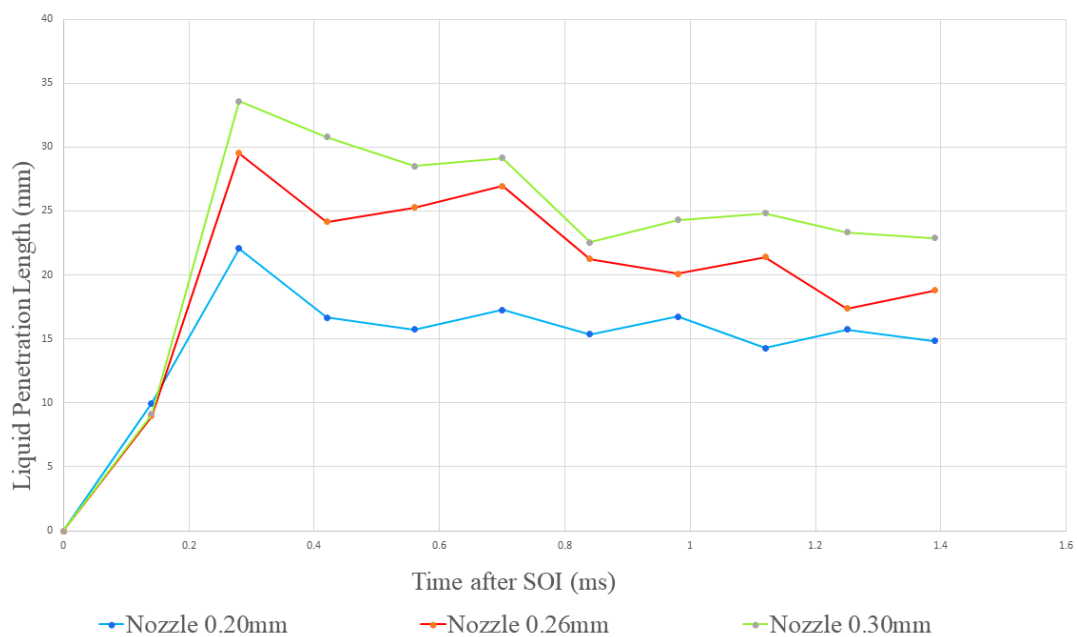


Figure 4.6. Variation of liquid penetration length for three different nozzle hole diameters.

The liquid penetration length is the measure of the speed and the distance penetrated by the fuel spray inside the combustion chamber. It significantly affects the fuel-air mixing process by affecting air utilization. In some engines, the fuel spray is required to impinge on the cylinder wall that is at an elevated temperature in the presence of an air swirl. However, for multi-injection diesel engines, the over-penetration of the fuel spray

impingement on the wall is prevented. This resulted in the impingement of fuel on the relatively cooler wall surfaces. The over-penetration causes a lower rate of air-fuel mixing and thus increases the emissions caused due to unburned or partially burned species. On the other hand, under-penetration of the fuel spray resulted in improper utilization of air for mixing with the fuel. This is because the air present in the cylinder does not get in contact with the fuel. Due to this, a proper understanding of the penetration length is required for the fuel sprays. Figure 4.6 portrays the varying trend of liquid penetration length from the start of injection for three nozzle hole diameters. The results obtained are similar to the findings in previous experimental work [97]. The increase in the penetration length with the increased diameters confirms the effect of the breakup model used in the study. The larger nozzle hole diameter results in the formation of larger spray zone width and larger spray cone zone.

4.4.3.2 Break-up Length

The atomization process is a complex break-up phenomenon that consists of various spatial and temporal scales. One of the spatial scales is known as the break-up length that defines the length of the continuous fuel jet passing through the nozzle exit. During the atomization process, the spray disintegrates into the smaller droplets. To study this process, a better understanding of the break-up length is required. The basic mechanism of the atomization process is divided into the primary and the secondary atomization process [101].

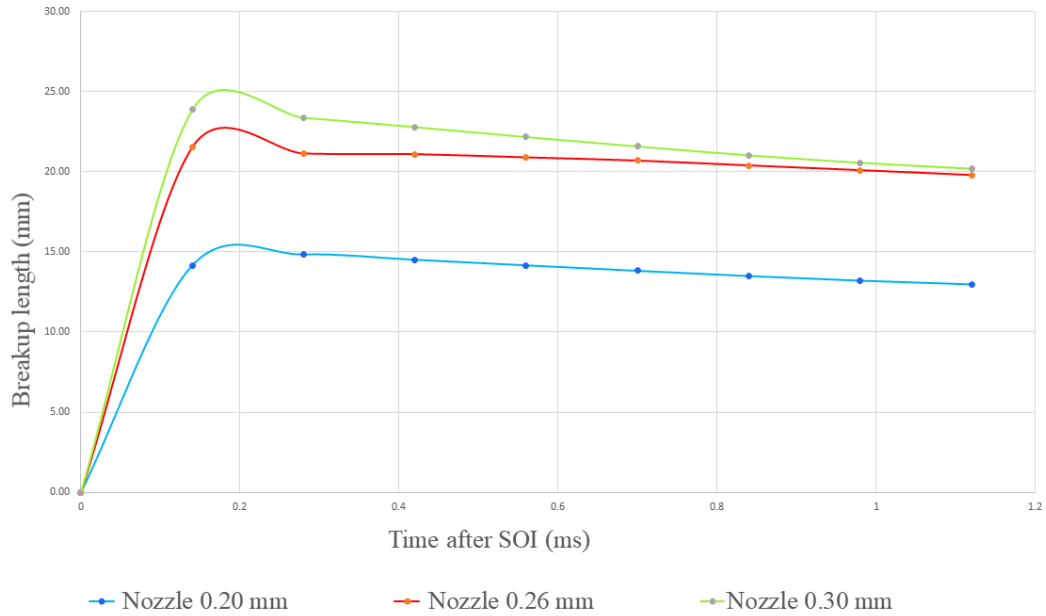


Figure 4.7. Variation of breakup length for three different nozzle hole diameters.

The primary atomization initiated instantly just after the exit of the injector nozzle. During this process, various destabilizing forces act on the interface of the mixture resulted in the breaking up of the continuous stream of liquid into the different liquid fragments. At the downstream of the nozzle exit, the secondary atomization process occurs because of the interruption in the continuity of the liquid stream. This causes the liquid fragments to break further into the smaller droplets and continues till the stable droplets are formed. The break-up length is the measure of the spatial extent of the primary atomization process. Figure 4.7 presents the variation of break-up length from the start of injection for three nozzle hole diameters. The results obtained are similar to the findings in previous literature [102]. The similarity of the variation break-up length between simulation and experimental results shows that the gas jet break-up models are properly set. The variation in break-up length for different nozzle diameters confirms the effect of the breakup model used in the study.

4.4.3.3 Sauter Mean Diameter (SMD)

Some studies on engine combustion, emission, and spray characteristics of a CRDI diesel engine with variable nozzle geometry using ANSYS

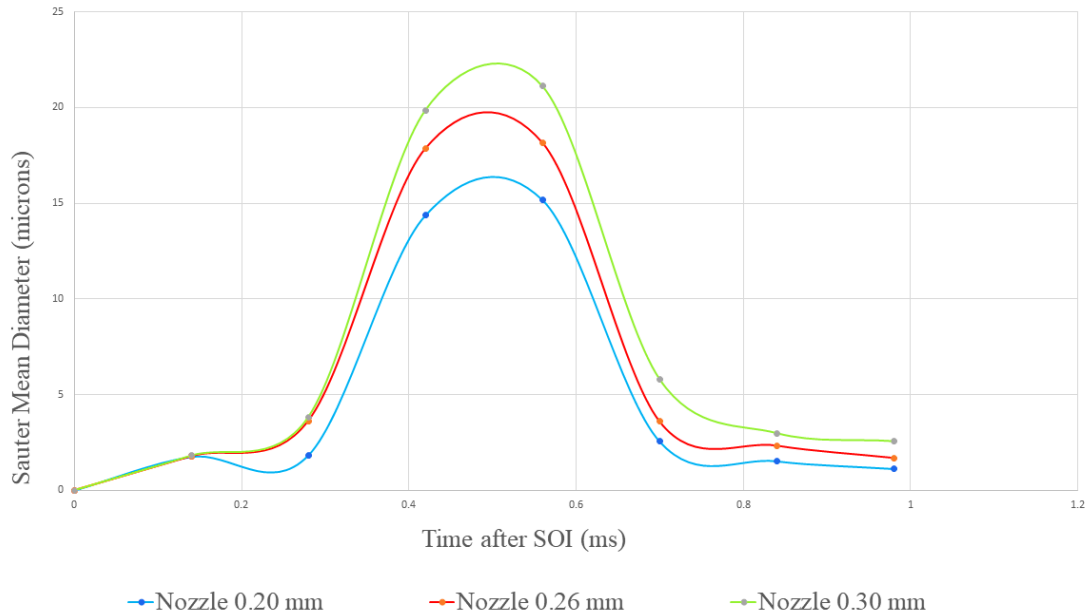


Figure 4.8. Variation of SMD for three different nozzle hole diameters.

The fuel is injected from the nozzle in the form of a spray that includes fuel droplets of varying sizes. The average size of these droplets is statistically calculated which is known as the SMD. [31] found that the size of the fuel droplets varies with the injection pressure, amount of fuel injected, and density of the air-entrained. The process of atomization ensures that the liquid fuel is disintegrated into the smaller droplets thus forming a larger surface area. This large surface area formation makes sure that the liquid fuel gets evaporated. The SMD is mathematically defined as the volume-to-surface mean diameter that measures how effectively the liquid fuel undergoes the atomization process. The variation of the SMD from the start of injection for three nozzle hole diameters is portrayed in Figure 4.8. The result represents the transition of droplet size after the start of injection. The trend obtained for the SMD is similar to the findings in previous literature [103]. The smaller droplet size improves the atomization process that ensures the rapid vaporization of the fuel droplets. The rapid vaporization process improves the overall combustion process inside the cylinder. However, as the

nozzle hole diameter increases, the SMD also increases because of the formation of larger size fuel droplets. [101] has shown that lower combustion rates and longer combustion duration are observed when the SMD increases.

4.3 Summary

In this chapter, the combustion, emission, and spray characteristics of a diesel engine have been analyzed. The result shows that the RNG $k - \varepsilon$ model is able to predict the flow characteristics. The results obtained are also verified using the previous studies. The CFD simulations were performed for different nozzle hole diameters utilizing the same turbulent model. The spray model is also found to be effective in the study.

CHAPTER 5

CONCLUSION AND FUTURE WORK

5.1 CONCLUSION

The present study utilizes the CFD simulation software to obtain accurate combustion, emission, and spray characteristics. The CFD model employed in the study includes the submodels such as turbulent model, spray break-up model, and combustion. The result shows that the CFD model employed in the study has effectively predicted the characteristics of the diesel engine.

The conclusions from the research study are outlined as:

1. The experimental results from the diesel engine have successfully validated the results obtained from the CFD. The relative error for in-cylinder pressure at 5 °bTDC and 3 °aTDC was found to be 2.39% and 2.58%, respectively, between the numerical and experimental analysis. The relative error for AHRR at 12° bTDC and 5 °aTDC was found to be 6.89% and 8.54%, respectively. The relative errors are found to be within the range.
2. The CFD model has effectively predicted the in-cylinder pressure variation with respect to the crank angle for different nozzle hole diameters. The peak in-cylinder pressure was found maximum for 0.20 mm nozzle hole diameter. Also, the peak in-cylinder reduced by 8.31% and 11.85% respectively, for 0.26 mm and 0.30 mm diameter as compared to 0.20 mm nozzle hole diameter.
3. The CFD model has also effectively predicted the variation in the AHRR with respect to the crank angle for different nozzle hole diameters. The peak heat release rate was found maximum for 0.20 mm nozzle hole diameter. The peak

heat release reduced by 11.82% and 32.55%, respectively for 0.26 mm and 0.30 mm diameter compared to 0.20 mm nozzle hole diameter.

4. The HC and CO emissions are found higher for larger nozzle hole diameter. The HC emissions are increased by 29.90% and 60.13%, respectively for 0.26 mm and 0.30 mm diameter compared to the 0.20 mm nozzle hole diameter. Similarly, the CO emissions increased by 0.65% and 5.08% respectively for 0.26 mm and 0.30 mm diameter compared to 0.20 mm nozzle hole diameter.
5. The NO_x emissions are found lower for larger nozzle hole diameter. The NO_x emissions are decreased by 41.18% and 70.58% respectively for 0.26 mm and 0.30 mm diameter compared to the 0.20 mm nozzle hole diameter.
6. The liquid penetration length, break-up length, and SMD of the diesel fuel are found to increase with the increase in the nozzle diameter.

5.2 SCOPE FOR FUTURE WORK

According to the result obtained from this study, the following recommendations can be outlined for future work:

1. Future researchers can focus on using the ANSYS Forte module on other diesel-like fuels and compare the result with the experimental results.
2. The current CFD modeling approach can be used for simulating the engines running at different operative conditions and validate the result with the experimental results.
3. The spray characteristics can further be analyzed using the ANSYS Enight module which enables the visual analysis of the fuel spray at a different crank angle.

4. The increase in the NO_x emissions with the increase in the nozzle hole diameter was observed for the present study. However, in the future, studies can also be carried out to reduce NO_x emission using techniques such as EGR.

REFERENCES

- [1] S. Baek, H. Lee, and K. Lee, "Fuel efficiency and exhaust characteristics of turbocharged diesel engine equipped with an electric supercharger," *Energy*, vol. 214, p. 119049, Jan. 2021.
- [2] J. Wang, X. Duan, W. Wang, J. Guan, Y. Li, and J. Liu, "Effects of the continuous variable valve lift system and Miller cycle strategy on the performance behavior of the lean-burn natural gas spark ignition engine," *Fuel*, vol. 297, p. 120762, Aug. 2021.
- [3] S. Kanth, T. Ananad, S. Debbarma, and B. Das, "Effect of fuel opening injection pressure and injection timing of hydrogen enriched rice bran biodiesel fuelled in CI engine," *Int. J. Hydrogen Energy*, Jul. 2021.
- [4] Y. Wang, L. Liu, and M. Yao, "Experimental and numerical study on the impact of low-temperature reforming products of BD60 on engine combustion and emission characteristics," *Fuel*, vol. 288, p. 119621, Mar. 2021.
- [5] V. D. Chaudhari and D. Deshmukh, "Diesel and diesel-gasoline fuelled premixed low temperature combustion (LTC) engine mode for clean combustion," *Fuel*, vol. 266, p. 116982, Apr. 2020.
- [6] Z. Chen, J. He, H. Chen, L. Geng, and P. Zhang, "Comparative study on the combustion and emissions of dual-fuel common rail engines fueled with diesel/methanol, diesel/ethanol, and diesel/n-butanol," *Fuel*, vol. 304, p. 121360, Nov. 2021.
- [7] B. N. Agrawal, S. Sinha, A. V. Kuzmin, and V. A. Pinchuk, "Effect of vegetable oil share on combustion characteristics and thermal efficiency of

- diesel engine fueled with different blends,” *Therm. Sci. Eng. Prog.*, vol. 14, p. 100404, Dec. 2019.
- [8] J. B. Heywood, “DIESEL ENGINE COMBUSTION,” 2nd editio., New York: McGraw-Hill Education, 2018.
- [9] S. McAllister, J.-Y. Chen, and A. C. Fernandez-Pello, *Fundamentals of Combustion Processes*. 2011.
- [10] D. J. Patterson and N. A. Henein, *Emissions from combustion engines and their control*. United States: Ann Arbor Science, Ann Arbor, MI, 1981.
- [11] J. B. Heywood, *Internal Combustion Engine Fundamentals*. N. York: McGraw-Hill. 1988.
- [12] L. M. Avallone, “OBSERVATIONS FOR CHEMISTRY (IN SITU) | Resonance Fluorescence,” J. R. B. T.-E. of A. S. Holton, Ed. Oxford: Academic Press, 2003, pp. 1484–1490.
- [13] R. C. Flagan and J. H. Seinfeld, “Pollutant formation and Control in Combustion,” *Fundam. air Pollut. Eng.*, p. 168, 1988.
- [14] M. Semakula and P. F. Inambao, “The Formation, Effects and Control of Oxides of Nitrogen in Diesel Engines,” *Int. J. Appl. Eng. Res.*, vol. 13, no. 6, pp. 3200–3209, 2018.
- [15] Y. Ikeda, T. Nakajima, and E. Sher, *Air Pollution from Small Two-Stroke Engines and Technologies to Control It*. 1998.
- [16] F. F. Pischinger, “Introduction,” *Handb. Air Pollut. From Intern. Combust. Engines*, vol. 27, pp. 261–279, 1998.

- [17] T. Shudo, K. Omori, and O. Hiyama, “NO_x reduction and NO₂ emission characteristics in rich-lean combustion of hydrogen,” *Int. J. Hydrogen Energy*, vol. 33, no. 17, pp. 4689–4693, 2008.
- [18] R. Sindhu, G. Amba Prasad Rao, and K. Madhu Murthy, “Effective reduction of NO_x emissions from diesel engine using split injections,” *Alexandria Eng. J.*, vol. 57, no. 3, pp. 1379–1392, 2018.
- [19] K. S. Varde and D. M. Popa, “Diesel fuel spray penetration at high injection pressures,” *SAE Tech. Pap.*, 1983.
- [20] C. Baumgarten, “Mixture Formation in IC Engines,” pp. 215–230, 2006.
- [21] D. S. Nath and N. Kumar, “To investigate the variation in Swirl Ratio by changing the Valve Lift of an Internal Combustion Engine,” *IOP Conf. Ser. Mater. Sci. Eng.*, vol. 804, no. 1, pp. 0–7, 2020.
- [22] A. A. Hamidi and J. Swithenbank, “Processes and Spray Diagnostic Methods,” 1990.
- [23] R. D. Reitz and F. V. Bracco, “Mechanism of atomization of a liquid jet,” *Phys. Fluids*, vol. 25, no. 10, pp. 1730–1742, 1982.
- [24] E. N. Balles and J. B. Heywood, “Fuel-air mixing and diesel combustion in a rapid compression machine,” *SAE Tech. Pap.*, 1988.
- [25] J. B. Heywood, “FUEL SPRAY BEHAVIOR,” 2nd editio., New York: McGraw-Hill Education, 2018.
- [26] J. D. Naber and D. L. Siebers, “Effects of gas density and vaporization on penetration and dispersion of diesel sprays,” *SAE Tech. Pap.*, no. 412, 1996.

- [27] V. K. Sharma, M. Mohan, and C. Mouli, “Effect of intake swirl on the performance of single cylinder direct injection diesel engine,” *IOP Conf. Ser. Mater. Sci. Eng.*, vol. 263, no. 6, 2017.
- [28] K. Fukuda, A. Ghasemi, R. Barron, and R. Balachandar, “An open cycle simulation of di diesel engine flow field effect on spray processes,” *SAE Tech. Pap.*, no. April, 2012.
- [29] G. L. Martinez *et al.*, “Measurement of Sauter mean diameter in diesel sprays using a scattering–absorption measurement ratio technique,” *Int. J. Engine Res.*, vol. 20, no. 1, pp. 6–17, 2019.
- [30] Y. Y. Gong, L. H. You, and X. M. Liang, “An investigation on droplet size distribution and evaporation of diesel fuel sprays at high injection pressure by using laser diagnostic technique,” *SAE Tech. Pap.*, 1992.
- [31] H. Hiroyasu and T. Kadota, “Fuel droplet size distribution in diesel combustion chamber,” *SAE Tech. Pap.*, pp. 2615–2624, 1974.
- [32] L. Geng, Y. Wang, Y. Wang, and H. Li, “Effect of the injection pressure and orifice diameter on the spray characteristics of biodiesel,” *J. Traffic Transp. Eng. (English Ed.)*, vol. 7, no. 3, pp. 331–339, 2020.
- [33] X. Wei and H. Yong, “Improved semiempirical correlation to predict Sauter mean diameter for pressure-swirl atomizers,” *J. Propuls. Power*, vol. 30, no. 6, pp. 1628–1635, 2014.
- [34] J. Dernet, C. Hespe, S. Houillé, F. Foucher, and C. Mounäim-Rousselle, “Influence of fuel properties on the diesel injection process in nonvaporizing conditions,” *At. Sprays*, vol. 22, no. 6, pp. 461–492, 2012.

- [35] D. L. Siebers, “Scaling liquid-phase fuel penetration in diesel sprays based on mixing-limited vaporization,” *SAE Tech. Pap.*, no. 724, 1999.
- [36] IICT Policy Update, “India bharat stage VI emission standards,” *Int. Counc. Clean Transp.*, no. April, p. 10, 2016.
- [37] K. Mohiuddin, H. Kwon, M. Choi, and S. Park, “Experimental investigation on the effect of injector hole number on engine performance and particle number emissions in a light-duty diesel engine,” *Int. J. Engine Res.*, vol. 22, no. 8, pp. 2689–2708, 2021.
- [38] C. Nandakumar, V. Raman, C. G. Saravanan, M. Vikneswaran, S. Prasanna Raj Yadav, and M. Thirunavukkarasu, “Effect of nozzle hole geometry on the operation of kapok biodiesel in a diesel engine,” *Fuel*, vol. 276, p. 118114, Sep. 2020.
- [39] M. Walle Mekonen and N. Sahoo, “Combined effects of fuel injection pressure and injector nozzle holes on the performance of preheated palm oil methyl ester used in a diesel engine,” *Biofuels*, vol. 11, no. 1, pp. 19–35, 2020.
- [40] F. J. Salvador, J. M. Pastor, J. De la Morena, and E. C. Martínez-Miracle, “Computational study on the influence of nozzle eccentricity in spray formation by means of Eulerian Σ - Y coupled simulations in diesel injection nozzles,” *Int. J. Multiph. Flow*, vol. 129, p. 103338, Aug. 2020.
- [41] V. S. Yaliwal, N. R. Banapurmath, N. M. Gireesh, R. S. Hosmath, T. Donateo, and P. G. Tewari, “Effect of nozzle and combustion chamber geometry on the performance of a diesel engine operated on dual fuel mode using renewable fuels,” *Renew. Energy*, vol. 93, pp. 483–501, Aug. 2016.

- [42] G. Vairamuthu, S. Sundarapandian, C. Kailasanathan, and B. Thangagiri, “Experimental investigation on the effects of cerium oxide nanoparticle on Calophyllum inophyllum (Punnai) biodiesel blended with diesel fuel in DI diesel engine modified by nozzle geometry,” *J. Energy Inst.*, vol. 89, no. 4, pp. 668–682, Nov. 2016.
- [43] G. Suresh, H. C. Kamath, and N. R. Banapurmath, “Effects of injection timing, injector opening pressure and nozzle geometry on the performance of cottonseed oil methyl ester-fuelled diesel engine,” *Int. J. Sustain. Eng.*, vol. 7, no. 1, pp. 82–92, 2014.
- [44] C. Sayin, M. Gumus, and M. Canakci, “Influence of injector hole number on the performance and emissions of a DI diesel engine fueled with biodiesel–diesel fuel blends,” *Appl. Therm. Eng.*, vol. 61, no. 2, pp. 121–128, Nov. 2013.
- [45] P. K. Karra and S. C. Kong, “Experimental study on effects of nozzle hole geometry on achieving low diesel engine emissions,” *J. Eng. Gas Turbines Power*, vol. 132, no. 2, pp. 1–10, 2010.
- [46] D. T. Montgomery, M. Chan, C. T. Chang, P. V. Farrell, and R. D. Reitz, “Effect of injector nozzle hole size and number on spray characteristics and the performance of a heavy duty D.I. diesel engine,” *SAE Tech. Pap.*, no. 412, 1996.
- [47] A. J. Deokar and P. A. Harari, “Effect of injection pressure, injection timing and nozzle geometry on performance and emission characteristics of diesel engine operated with thevetia peruviana biodiesel,” *Mater. Today Proc.*, 2021.
- [48] K. M. Akkoli *et al.*, “Effect of injection parameters and producer gas derived from redgram stalk on the performance and emission characteristics of a diesel

- engine,” *Alexandria Eng. J.*, vol. 60, no. 3, pp. 3133–3142, 2021.
- [49] U. Rajak, P. Nashine, and T. Nath Verma, “Numerical study on emission characteristics of a diesel engine fuelled with diesel-spirulina microalgae-ethanol blends at various operating conditions,” *Fuel*, vol. 262, no. September 2019, p. 116519, 2020.
- [50] S. K. Nayak, P. C. Mishra, and M. M. Noor, “Simultaneous reduction of nitric oxide and smoke opacity in TDI dual fuel engine fuelled with calophyllum-diesel blends and waste wood chip gas for modified inlet valve and injector nozzle geometry,” *Energy*, vol. 189, no. x, p. 116238, 2019.
- [51] M. M. Shivashimpi, S. A. Alur, S. N. Topannavar, and B. M. Dodamani, “Combined effect of combustion chamber shapes and nozzle geometry on the performance and emission characteristics of C.I. engine operated on Pongamia,” *Energy*, vol. 154, pp. 17–26, 2018.
- [52] S. Dong, C. Yang, B. Ou, H. Lu, and X. Cheng, “Experimental investigation on the effects of nozzle-hole number on combustion and emission characteristics of ethanol/diesel dual-fuel engine,” *Fuel*, vol. 217, no. July 2017, pp. 1–10, 2018.
- [53] F. Leach, R. Ismail, and M. Davy, “Engine-out emissions from a modern high speed diesel engine – The importance of Nozzle Tip Protrusion,” *Appl. Energy*, vol. 226, pp. 340–352, Sep. 2018.
- [54] R. Payri, J. P. Viera, V. Gopalakrishnan, and P. G. Szymkowicz, “The effect of nozzle geometry over ignition delay and flame lift-off of reacting direct-injection sprays for three different fuels,” *Fuel*, vol. 199, pp. 76–90, Jul. 2017.

- [55] R. Payri, J. P. Viera, V. Gopalakrishnan, and P. G. Szymkowicz, “The effect of nozzle geometry over internal flow and spray formation for three different fuels,” *Fuel*, vol. 183, pp. 20–33, Nov. 2016.
- [56] S. N. Kane, A. Mishra, and A. K. Dutta, “Preface: International Conference on Recent Trends in Physics (ICRTP 2016),” *J. Phys. Conf. Ser.*, vol. 755, no. 1, 2016.
- [57] S. Lahane and K. A. Subramanian, “Impact of nozzle holes configuration on fuel spray, wall impingement and NO_x emission of a diesel engine for biodiesel-diesel blend (B20),” *Appl. Therm. Eng.*, vol. 64, no. 1–2, pp. 307–314, 2014.
- [58] S. Som, A. I. Ramirez, D. E. Longman, and S. K. Aggarwal, “Effect of nozzle orifice geometry on spray, combustion, and emission characteristics under diesel engine conditions,” *Fuel*, vol. 90, no. 3, pp. 1267–1276, Mar. 2011.
- [59] S. W. Park and R. D. Reitz, “Modeling the effect of injector nozzle-hole layout on diesel engine fuel consumption and emissions,” *J. Eng. Gas Turbines Power*, vol. 130, no. 3, pp. 1–10, 2008.
- [60] D. T. Hountalas, T. C. Zannis, G. C. Mavropoulos, V. Schwarz, J. Benajes, and C. A. Gonzalez, “Use of a multi-zone combustion model to interpret the effect of injector nozzle hole geometry on HD di diesel engine performance and pollutant emissions,” *SAE Tech. Pap.*, vol. 2005, no. x, 2005.
- [61] M. Medina, A. Bautista, M. Wooldridge, and R. Payri, “The effects of injector geometry and operating conditions on spray mass, momentum and development using high-pressure gasoline,” *Fuel*, vol. 294, p. 120468, Jun. 2021.

- [62] N. Watanabe, N. Kurimoto, K. Serizawa, M. Yoshino, S. Skeen, and L. M. Pickett, "Identification of significant design factors for diesel spray combustion control through comprehensive experiments with various multi-hole nozzle internal geometries," *Int. J. Engine Res.*, p. 1468087420983755, Jan. 2021.
- [63] R. Balz, G. Bernardasci, B. von Rotz, and D. Sedarsky, "Influence of nozzle geometry on spray and combustion characteristics related to large two-stroke engine fuel injection systems," *Fuel*, vol. 294, p. 120455, Jun. 2021.
- [64] P. Mano Alexander, S. Nandhakumar, S. Seenivasan, N. A. Ashfaq Ahamed, and P. Raj Kumar, "Optimal orientation of injectors for efficient spray pattern of fuel flow in a diesel engine," *Mater. Today Proc.*, vol. 37, no. Part 2, pp. 2890–2896, Jan. 2021.
- [65] W. Huang, S. Moon, Y. Gao, J. Wang, D. Ozawa, and A. Matsumoto, "Hole number effect on spray dynamics of multi-hole diesel nozzles: An observation from three- to nine-hole nozzles," *Exp. Therm. Fluid Sci.*, vol. 102, pp. 387–396, Apr. 2019.
- [66] Z. Chen *et al.*, "Experimental study on the effect of nozzle geometry on string cavitation in real-size optical diesel nozzles and spray characteristics," *Fuel*, vol. 232, pp. 562–571, Nov. 2018.
- [67] Z. He, G. Guo, X. Tao, W. Zhong, X. Leng, and Q. Wang, "Study of the effect of nozzle hole shape on internal flow and spray characteristics," *Int. Commun. Heat Mass Transf.*, vol. 71, pp. 1–8, Feb. 2016.
- [68] C. J. Rutland, "Large-eddy simulations for internal combustion engines - A review," *Int. J. Engine Res.*, vol. 12, no. 5, pp. 421–451, 2011.

- [69] Y. Wang *et al.*, “Evaluation and Validation of Large-Eddy-Simulation (LES) for Gas Jet and Sprays.” SAE International, 2017.
- [70] C. W. Tsang, M. F. Trujillo, and C. J. Rutland, “Large-eddy simulation of shear flows and high-speed vaporizing liquid fuel sprays,” *Comput. Fluids*, vol. 105, pp. 262–279, 2014.
- [71] M. G. Kazimardanov, S. V. Mingalev, T. P. Lubimova, and L. Y. Gomzikov, “Simulation of Primary Film Atomization Due to Kelvin–Helmholtz Instability,” *J. Appl. Mech. Tech. Phys.*, vol. 59, no. 7, pp. 1251–1260, 2018.
- [72] C. W. Hirt, A. A. Amsden, and J. L. Cook, “An arbitrary Lagrangian-Eulerian computing method for all flow speeds,” *J. Comput. Phys.*, vol. 14, no. 3, pp. 227–253, 1974.
- [73] W. E. Pracht, “Calculating three-dimensional fluid flows at all speeds with an Eulerian-Lagrangian computing mesh,” *J. Comput. Phys.*, vol. 17, no. 2, pp. 132–159, Feb. 1975.
- [74] Ansys Inc., “Forte Theory Manual,” no. January, pp. 1–29, 2020.
- [75] T. F. Su, M. A. Patterson, R. D. Reitz, and P. V. Farrell, “Experimental and numerical studies of high pressure multiple injection sprays,” *SAE Tech. Pap.*, no. 412, 1996.
- [76] J. Beale and R. Reitz, “Modeling spray atomization with the KH-RT hybrid model.” pp. 623–650, 1999.
- [77] C. S. Lee and S. W. Park, “An experimental and numerical study on fuel atomization characteristics of high-pressure diesel injection sprays,” *Fuel*, vol. 81, no. 18, pp. 2417–2423, 2002.

- [78] Z. HAN and R. D. REITZ, “Turbulence Modeling of Internal Combustion Engines Using RNG κ - ϵ Models,” *Combust. Sci. Technol.*, vol. 106, no. 4–6, pp. 267–295, Jan. 1995.
- [79] Z. Han and R. D. Reitz, “A temperature wall function formulation for variable-density turbulent flows with application to engine convective heat transfer modeling,” *Int. J. Heat Mass Transf.*, vol. 40, no. 3, pp. 613–625, Feb. 1997.
- [80] A. B. Liu, D. Mather, and R. D. Reitz, “Modeling the effects of drop drag and breakup on fuel sprays,” *SAE Tech. Pap.*, no. 412, 1993.
- [81] S. C. Kong and R. D. Reitz, “Multidimensional modeling of diesel ignition and combustion using a multistep kinetics model,” *J. Eng. Gas Turbines Power*, vol. 115, no. 4, pp. 781–789, 1993.
- [82] S. C. Kong, Z. Han, and R. D. Reitz, “The development and application of a diesel ignition and combustion model for multidimensional engine simulation,” *SAE Tech. Pap.*, no. 412, 1995.
- [83] Z. Han, A. Uludogan, G. J. Hampson, and R. D. Reitz, “Mechanism of soot and NO_x emission reduction using multiple-injection in a diesel engine,” *SAE Tech. Pap.*, no. January 1996, 1996.
- [84] S. Mauro, R. Şener, M. Z. Gül, R. Lanzafame, M. Messina, and S. Brusca, “Internal combustion engine heat release calculation using single-zone and CFD 3D numerical models,” *Int. J. Energy Environ. Eng.*, vol. 9, no. 2, pp. 215–226, 2018.
- [85] D. N. Assanis, Z. S. Filipi, S. B. Fiveland, and M. Syrimis, “A methodology for cycle-by-cycle transient heat release analysis in a turbocharged direct injection

- diesel engine,” *SAE Tech. Pap.*, no. 724, 2000.
- [86] K. Siva Prasad, S. Srinivasa Rao, and V. R. K. Raju, “Effect of compression ratio and fuel injection pressure on the characteristics of a CI engine operating with butanol/diesel blends,” *Alexandria Eng. J.*, vol. 60, no. 1, pp. 1183–1197, Feb. 2021.
- [87] M. Hawi, H. Kosaka, S. Sato, T. Nagasawa, A. Elwardany, and M. Ahmed, “Effect of injection pressure and ambient density on spray characteristics of diesel and biodiesel surrogate fuels,” *Fuel*, vol. 254, no. June, p. 115674, 2019.
- [88] J. Liu, Q. Guo, J. Guo, and F. Wang, “Optimization of a diesel/natural gas dual fuel engine under different diesel substitution ratios,” *Fuel*, vol. 305, no. May, p. 121522, 2021.
- [89] J. Liu, H. Zhao, J. Wang, and N. Zhang, “Optimization of the injection parameters of a diesel/natural gas dual fuel engine with multi-objective evolutionary algorithms,” *Appl. Therm. Eng.*, vol. 150, no. November 2018, pp. 70–79, 2019.
- [90] A. Nerkar, “Optimization and Validation for Injector Nozzle Hole Diameter of a Single Cylinder Diesel Engine using GT-Power Simulation Tool,” *SAE Int. J. Fuels Lubr.*, vol. 5, no. 3, pp. 1372–1381, 2012.
- [91] R. J. Moffat, “Describing the uncertainties in experimental results,” *Exp. Therm. Fluid Sci.*, vol. 1, no. 1, pp. 3–17, 1988.
- [92] M. A. Mashkour and M. A. Mashkour Mustafa Hadi Ibraheem, “CFD Analysis of Petrol Internal Combustion Engine,” *J. Univ. Babylon Eng. Sci.*, no. 26, p. 2018, 2018.

- [93] M. Baratta, S. Chiriches, P. Goel, and D. Misul, “CFD modelling of natural gas combustion in IC engines under different EGR dilution and H₂-doping conditions,” *Transp. Eng.*, vol. 2, no. June, 2020.
- [94] R. Yang, G. Theotokatos, and D. Vassalos, “CFD modelling and numerical investigation of a large marine two-stroke dual fuel direct injection engine,” *Ships Offshore Struct.*, vol. 0, no. 0, pp. 1–13, 2021.
- [95] P. Bergstrand and I. Denbratt, “Diesel combustion with reduced nozzle orifice diameter,” *SAE Tech. Pap.*, no. 724, 2001.
- [96] M. Vijay Kumar, A. Veeresh babu, P. Ravi Kumar, and T. Manoj Kumar Dundi, “Influence of different nozzle hole orifice diameter on performance, combustion and emissions in a diesel engine,” *Aust. J. Mech. Eng.*, vol. 18, no. 2, pp. 179–184, 2020.
- [97] V. Kumbhar, A. K. Pandey, and A. Varghese, “Effect of fuel injector nozzle hole diameter on emissions of CAT 3401 diesel engine using CONVERGETM CFD,” *Int. J. Eng. Adv. Technol.*, vol. 8, no. 6, pp. 927–932, 2019.
- [98] EPA, “Nitrogen oxides (NO_x), why and how they are controlled,” *Epa-456/F-99-006R*, no. November, p. 48, 1999.
- [99] A. M. Mellor, J. P. Mello, K. P. Duffy, W. L. Easley, and J. C. Faulkner, “Skeletal Mechanism for NO_x Chemistry in Diesel Engines Reprinted From: New Techniques in SI and Diesel Engine Modeling (SP-1366) International Spring Fuels and Lubricants Meeting and Exposition Dearborn, Michigan,” no. x, 2018.
- [100] L. Anetor, C. Odetunde, and E. E. Osakue, “Computational Analysis of the

Extended Zeldovich Mechanism,” *Arab. J. Sci. Eng.*, vol. 39, no. 11, pp. 8287–8305, 2014.

[101] A. H. Lefebvre and V. G. McDonnell, *Atomization and Sprays, Second Edition*. 2017.

[102] S. Wu, M. Meinhart, B. Petersen, J. Yi, and M. Wooldridge, “Breakup characteristics of high speed liquid jets from a single-hole injector,” *Fuel*, vol. 289, p. 119784, Apr. 2021.

[103] C. Yao, P. Geng, Z. Yin, J. Hu, D. Chen, and Y. Ju, “Impacts of nozzle geometry on spray combustion of high pressure common rail injectors in a constant volume combustion chamber,” *Fuel*, vol. 179, no. January, pp. 235–245, 2016.

Publication

V. Singh and N. Kumar, “Numerical investigation of the effect of nozzle hole diameter on the combustion, emission, and spray characteristics in a diesel engine,” *Energy Sources, Part A Recover. Util. Environ. Eff.*, pp. 1–18, Sep. 2021.